SRB and the extracts of *Zingiber officinale* and *Cinnamomum cassia* have previously been reported to have beneficial effects against hyperlipidemia, SRB did not affect serum total cholesterol level in the present study. This indicates that SRB could decrease serum total cholesterol level in a hyperlipidemia model (Chung et al., 2003; Yoshie et al., 2001) or *in vitro* (Kannappan et al., 2006; Matsuda et al., 2009), but not in an ovariectomy model.

Several reports show that IL-6 and other cytokines mediate bone loss induced by estrogen deficiency (Jika et al., 1992; Poli et al., 1994). In the presence of estrogen, IL-6 expression is suppressed, but its level increases in the absence of estrogen, and several clinical studies have shown high serum IL-6 levels among postmenopausal women (Pacifici et al., 1991). IL-6 is suggested to be a primary mediator of bone resorption through induction of osteoclastogenesis (Flanagan et al., 1995). IL-6 upregulation has an important role in the development of osteoporosis in ovariectomized mice and can be inhibited by androgen or IL-6 neutralizing antibody (Bellido et al., 1995). The present study showed that serum IL-6 levels in the SRB group were significantly lower than in the OVX group, suggesting that SRB can decrease serum IL-6 levels in this postmenopausal model.

Our histomorphometric results showed that the eroded surface (an indicator of osteoclast activity) was significantly smaller in the SRB group than in the OVX group. This lends support to the premise that SRB suppressed osteoclastogenesis by reducing serum IL-6 level. In our study, ovariectomized mice were not administered other therapies such as replacement estrogen therapy, which would have increased bone density and decreased serum IL-6. In that sense, we did not use any positive controls in this experiment. However, the comparison of bone and serum data with the OVX group support the idea that administration of SRB in a postmenopausal-osteoporosis model had an effect on preventing loss of bone volume and suppressing serum IL-6 levels.

Expression of IL-6 is largely controlled by nuclear factor-κB (NFκB) (Libermann and Baltimore, 1990). NFκB is an inducible dimeric transcription factor that belongs to the Rel/NFκB family of transcription factors. In resting cells, NFκB is sequestered in the cytoplasm by IκB proteins. Stimulus-mediated phosphorylation and subsequent proteolytic degradation of IκB allows the release and nuclear translocation of NFκB, where it transactivates a number of target genes. Recently, it was reported that saikosaponin, a principal component of SRB, inhibited T cell activation via the suppression of NFκB (Leung et al., 2005). Dang et al. (2007) reported that saikosaponin attenuated CCl_4-induced hepatic fibrosis via downregulation of TNFα, IL-6, and NFκB expression. Thus, one of the mechanisms by which SRB prevents the development of bone loss might be suppression of the expression of IL-6 via NFκB inactivation. Extracts of *Cinnamomum cassia*, *Zingiber officinale* and *Panax ginseng*, which represent the principal components of SRB, reportedly suppress osteoclastogenesis (Han et al., 2007; Liu et al., 2009; Sung et al., 2009; Tsuji-Naito, 2008). Incorporating these herbal medicines would thus also contribute to the prevention of bone loss.

Conclusions

We showed that SRB can prevent loss of bone volume and suppress serum IL-6 level in a postmenopausal model. Our results suggest that SRB deserves further investigation as a therapeutic option for treatment of postmenopausal osteoporosis.

Acknowledgments

We would like to thank Drs. Masafumi Kashii and Junko Murai for their helpful advice on the OVX experiment, and Yasuo Tsukamoto, Yousuke Hashimoto, Akitoshi Asami and Naoko Hattori for their excellent pharmacological advice.

References

Barrett-Connor, E., Mosca, L., Collins, P., Geiger, M.J., Grady, D., Kornitzer, M., McNabb, M.A., Wenger, N.K., Raloxifene Use for The Heart (RUTH) Trial Investigators, 2006. Effects of raloxifene on cardiovascular events and breast cancer in postmenopausal women. The New England Journal of Medicine 13,355 (2), 125–137.

Bellido, T., Jilka, R.L., Boyce, B.F., Girasole, G., Broxmeyer, H., Dalrymple, S.A., Murray, R., Manolagas, S.C., 1995. Regulation of interleukin-6, osteoclastogenesis, and bone mass by androgens: the role of the androgen receptor. The Journal of Clinical Investigation 95 (6), 2886–2895.

Chae, H.J., Kang, J.S., Kim, J.H., Kim, C.W., Yoo, S.K., Shin, T.Y., Choi, B., Kim, H.M., Kim, H.R., 2001. Antiosteoporotic activity of Dae-Bo-Won-Chun in ovariectomized rats. Phytotherapy Research 15 (1), 53–57.

Chen, H., Emura, S., Isono, H., Shoumura, S., 2005. Effects of traditional Chinese medicine on bone loss in SAMP6: a murine model for senile osteoporosis. Biological & Pharmaceutical Bulletin 28 (5), 865–869.

Chung, H.J., Maruyama, I., Tani, T., 2003. Saiko-ka-ryu-kotsu-borei-to inhibits intimal thickening in carotid artery after balloon endothelial denudation in cholesterol-fed rats. Boilogical & Pharmaceutical Bulletin 26 (1), 56–60.

Cui, L., Wu, T., Deng, Y.Y., Ai, C.M., Chen, H.Q., 2004. Tanshinone prevents cancellous bone loss induced by ovariectomy in rats. Acta Pharmacologica Sinica 25 (5), 678–684.

Dang, S.S., Wang, B.F., Cheng, Y.A., Song, P., Liu, Z.G., Li, Z.F., 2007. Inhibitory effects of saikosaponin-d on CCl4-induced hepatic fibrogenesis in rats. World Journal of Gastroenterology 13 (4), 557–563.

Delmas, P.D., Bjarnason, N.H., Mitlak, B.H., Ravoux, A.C., Shah, A.S., Huster, W.J., Draper, M., Christiansen, C., 1997. Effects of raloxifene on bone mineral density, serum cholesterol concentrations, and uterine endometrium in pistmenopausal women. The New England Journal of Medicine 4, 1641–1647.

Edwards, C.J., Hart, D.J., Spector, T.D., 2000. Oral statins and increased bone-mineral density in postmenopausal women. Lancet 355 (9222), 2218–2219.

Flanagan, A.M., Stow, M.D., Williams, R., 1995. The effect of inteleukin-6 and soluble interleukin-6 receptor protein on the bone resorptive activity of human osteoclasts generated in vitro. The Journal of Pathology 176 (3), 289–297.

Han, S.Y., Lee, J.R., Kwon, Y.K., Jo, M.J., Park, S.J., Kim, S.C., Lee, H.S., Ku, S.K., 2007. Ostreae Testa prevent ovariectomy-induced bone loss in mice by osteoblast activations. Journal of Ethnopharmacology 114 (3), 400–405.

Hill, K., 1996. The demography of menopause. Maturitas 23 (2), 113–127.

Hidaka, S., Okamoto, Y., Nakajima, K., Suekawa, M., Liu, S.Y., 1997. Preventive effects of traditional Chinese (Kampo) medicines on experimental osteoporosis induced by ovariectomy in rats. Calcified Tissue International 61 (3), 239–246.

Hidaka, S., Okamoto, Y., Yamada, Y., Kon, Y., Kimura, T., 1999. A Japanese herbal medicine, Chujo-to, has a benefical effect on osteoporosis in rats. Phytotherapy Research 13 (1), 14–19.

Hodsman, A.B., 2001. Fragility fractures in dialysis and transplant patients. Is it osteoporosis, and how should it be treated? Peritoneal Dialysis International 21 (Suppl. 3), S247–S255.

Jika, R.L., Hangoc, G., Girasole, G., Passeri, G., Williams, D.C., Abrams, J.S., Boyce, B., Broxmeyer, H., Manolagas, S.C., 1992. Increased osteoclast debelopment after estrogen loss: mediation by interleukin-6. Science 257 (5066), 88–91.

Kannappan, S., Jayaraman, T., Rajasekar, P., Ravichandran, M.K., Anuradha, C.V., 2006. Cinnamon bark extract improves glucose metabolism and lipid profile in the fructose-fed rat. Singapore Medical Journal 47 (10), 858–863.

Ke, H.Z., Chen, H.K., Qi, H., Pirie, C.M., Simmons, H.A., Ma, Y.F., Thompson, D.D., 1995. Effects of droloxifene on prevention of cancellous bone loss and bone turnover in the axial skeleton of aged, ovariectomized rats. Bone 17, 491–496.

Leung, C.Y., Liu, L., Wong, R.N., Zeng, Y.Y., Li, M., Zhou, H., 2005. Saikosaponin-d inhibits T cell activation through the modulation of PKCtheta, JNK, and NF-kappaB transcription factor. Biochemical and Biophysical Research Communications 338 (4), 1920–1927.

Li, H., Miyahara, T., Tezuka, Y., Namba, T., Nemoto, N., Tonami, S., Seto, H., Tada, T., Kadota, S., 1998. The effect of Kampo formulae on bone resorption in vitro and in vivo.1. Active constituents of Tsu-kan-gan. Biological Pharmaceutical Bulletin 21 (12), 1322–1326.

Li, H., Miyahara, T., Tezuka, Y., Namba, T., Suzuki, T., Dowaki, R., Watanabe, M., Nemoto, N., Tonami, S., Seto, H., Kadota, S., 1999. The effect of Kampo formulae on bone resorption in vitro and in vivo. 2. Detailed study of berberine. Biological & Pharmaceutical Bulletin 22 (4), 391–396.

Libermann, T.A., Baltimore, D., 1990. Activation of interleukin-6 gene expression through the NF-kappa B transcription Factor. Molecular and Cellular Biology 10 (5), 2327–2334.

Liu, J., Shiono, J., Shimizu, K., Yu, H., Zhang, C., Jin, F., Kondo, R., 2009. 20(R)-ginsenoside Rh2, not 20(S), is a selective osteoclastgenesis inhibitor without

any cytotoxicity. Bioorganic & Medical Chemistry Letters 19 (12), 3320–3323.
Matsuda, A., Wang, Z., Takahashi, S., Tokuda, T., Miura, N., Hasegawa, J., 2009. Upregulation of mRNA of retinoid binding protein and fatty acid binding protein by cholesterol enriched-diet and effect of ginger on lipid metabolism. Life Science 84 (25–26), 903–907.
Melton III, L.J., Kan, S.H., Frye, M.A., Wahner, H.W., O'Fallon, W.M., Riggs, B.L., 1989. Epidemiology of vertebral fractures in woman. American Journal of Epidemiology 129 (5), 1000–1011.
Mundy, G., Garrett, R., Harris, S., Chan, J., Chen, D., Rossini, G., Boyce, B., Zhao, M., Gutierrez, G., 1999. Stimulation of bone formation in vitro and in rodents by statins. Science 286 (5446), 1946–1949.
Okamoto, Y., Hidaka, S., Yamada, Y., Ouchi, K., Miyazaki, K., Liu, S.Y., 1998. Thermal analysis of bones from ovariectomized rats. Journal of Biomedical Materials Research 41 (2), 221–226.
Pacifici, R., Brown, C., Puscheck, E., Friedrich, E., Slatopolsky, E., Maggio, D., McCracken, R., Avioli, L.V., 1991. Effect of surgical menopause and estrogen replacement on cytokine release from human blood mononuclear cells. Proceedings of the National Academy of Sciences of the Unites States of America 88 (12), 5134–5138.
Perfitt, A.M., Drezner, M.K., Glorieux, F.H., Kanis, J.A., Malluche, H., Meunier, P.J., Ott, S.M., Recker, R.R., 1987. Bone histomorphometry: standardization of nomenclature, symbols, and units. Report of the ASBMR Histrmorphometry Nomenclature Committee. Journal of Bone and Mineral Reseach 2 (6), 595–610.
Poli, V., Balena, R., Fattori, E., Markatos, A., Yamamoto, M., Tanaka, H., Ciliberto, G., Rodan, G.A., Costantini, F., 1994. Interleukin-6 deficient mice are protected from bone loss caused by estrogen depletion. The EMBO Journal 13 (5), 1189–1196.
Poole, K.E., Compston, J.E., 2007. Osteoporosis and its management. BMJ 16, 1251–1256.
Ray, W.A., Daugherty, J.R., Griffin, M.R., 2002. Lipid-lowering agents and the risk of hip fracture in a Medicaid population. Injury Prevention 8 (4), 276–279.
Riggs, B.L., Melton 3rd, L.J., 1995. The worldwide problem of osteoporosis: insights afforded by epidemiology. Bone 17 (5), 505S–511S.
Ruggiero, S.L., Mehrotra, B., Rosenberg, T.J., Engroff, S.L., 2004. Osteonecrosis of the jaws associated with the use of bisphosphonates: a review if 63 cases. Journal of Oral and Maxillofacial Surgery 62 (5), 527–534.
Shi, L., Tezuka, Y., Subehan, Ueda, J., Miyahara, T., Yin, J., Nobukawa, T., Kadota, S., 2006. Inhibitory effect of kampo medicines on bone resorption in vitro and preventive effect on bone loss in vivo. Journal of Traditional Medicines 23, 92–100.
Sung, B., Murakami, A., Oyajobi, B.O., Aggarwal, B.B., 2009. Zerumbone abolishes RANKL-induced NF-kappaB activation, inhibits osteoclastogenesis, and suppresses human breast cancer-induced bone loss inathymic nude mice. Cancer Research 69 (4), 1477–1484.
Tsuji-Naito, K., 2008. Aldehydic components of cinnamon bark extract suppresses RANKL-induced osteoclastogenesis through NFATc1 downregulation. Bioorganic & Medical Journal 16 (20), 9176–9183.
Turbi, C., Herrero-Beaumont, G., Acebes, J.C., Torrijos, A., Grana, J., Miquelez, R., Sacristan, J., Marin, F., 2004. Compliance and satisfaction with raloxifene versus alendronate for the treatment of postmenopausal osteoporosis in clinical practice: an open-label, prospective, nonrandomized, observational study. Clincal Therapeutics 26 (2), 245–256.
Wang, P.S., Solomon, D.H., Mogun, H., Avorn, J., 2000. HMG-CoA reductase inhibitors and the risk of hip fractures in elderly patients. JAMA 283 (24), 3211–3216.
Yamada, T., Satoh, S., Katoh, S., Mizuno, G., Yoshomura, M., Sakurai, I., 1998. Pathological analysis on the effects of traditional Chinese drugs in spontaneously hypertensive rats (SHR) aorta. Doumyakukouka 16, 999–1007.
Yao, X., Chen, H., Emura, S., Otake, N., Shoumura, S., 2007. Effects of hPTH (1-34) and Gosha-jinki-gan on the trabecular bone microarchitecture in ovariectomized rat tibia. Okajimas Folia Anatomica Japonica 83 (4), 107–113.
Yoshie, F., Iizuka, A., Kubo, M., Komatsu, Y., Matsumoto, A., Itakura, H., Takeda., H., Matsumiya, T., Kondo, K., 2001. Protective effects of saiko-ka-ryu-kotsu-boreito (Chai-Hu-Jia-Long-Gu-Mu-Li-Tang) against atherisclerosis in Kurosawa and Kusanagi-hypercholesterolemic (KHC) rabbits. Pharmacogical Research 43 (5), 481–488.

Clinical & Experimental Immunology
The Journal of Translational Immunology

Clinical and Experimental Immunology ORIGINAL ARTICLE doi:10.1111/j.1365-2249.2010.04163.x

TP53 mutations coincide with the ectopic expression of activation-induced cytidine deaminase in the fibroblast-like synoviocytes derived from a fraction of patients with rheumatoid arthritis

H. Igarashi,* J. Hashimoto,† T. Tomita,† H. Yoshikawa† and K. Ishihara*

**Department of Immunology and Molecular Genetics, Kawasaki Medical School, Kurashiki City, Okayama, and †Department of Orthopaedics, Osaka University Graduate School of Medicine, Suita City, Osaka, Japan*

Summary

Main features of rheumatoid arthritis (RA), hyperplasia of fibroblast-like synoviocytes (FLS) and joint destruction are caused by inflammatory cytokines produced in chronic autoimmune inflammation. Cell-intrinsic acquisition of tumour-like phenotypes of RA-FLS could also be responsible for the aggressive proliferation and invasion, which are supported by the fact that in some cases RA-FLS has mutations of a tumour suppressor gene *TP53*. However, the underlying molecular mechanism for *TP53* mutations in RA-FLS has not yet been clarified. Recently it has been reported that the non-lymphoid cells in the inflammatory tissues express ectopically the *activation-induced cytidine deaminase (AID)* gene that induces somatic hypermutations, not only at the immunoglobulin (Ig) gene variable regions in germinal centre B lymphocytes but also at coding regions in *TP53*. Real-time polymerase chain reaction (PCR) analyses revealed more than half (five of nine) of the RA-FLS lines we established showed the markedly increased expression of *AID*. *AID* transcription in RA-FLS was augmented by tumour necrosis factor (TNF)-α and even by physiological concentration of β-oestradiol that could not induce *AID* transcription in osteoarthritis-FLS. Furthermore, AID-positive RA-FLS presented a higher frequency of somatic mutations in *TP53*. Cytological and immunohistochemical analyses demonstrated clearly the ectopic expression of *AID* in the FLS at the RA synovium. These data suggested strongly a novel consequence of RA; the ectopic expression of AID in RA-FLS causes the somatic mutations and dysfunction of *TP53*, leading to acquisition of tumour-like properties by RA-FLS.

Keywords: human, rheumatoid arthritis, somatic mutation, synoviocyte

Accepted for publication 24 February 2010
Correspondence: K. Ishihara, Department of Immunology and Molecular Genetics, Kawasaki Medical School, 577 Matsushima, Kurashiki City, Okayama 701-0192, Japan.
E-mail: ishihara-im@med.kawasaki-m.ac.jp

Introduction

Rheumatoid arthritis (RA) is a systemic autoimmune disease in which the joints are chronically inflamed and the cartilage and bone are destroyed by pannus formation, which is the invasion of cartilage and bone by proliferating fibroblast-like synoviocytes (FLS) [1–3]. The incidence of RA is correlated with certain human leucocyte antigen D-related (HLA-DR) haplotypes and the presence of autoantibodies, such as rheumatoid factor (RF) and anti-cyclic citrullinated peptide (CCP) antibody, suggesting strongly the involvement of the deregulated immune system; T helper type 17 (Th17), a novel helper T cell subset producing interleukin (IL)-17, has become a topic as a player in local inflammation driven by acquired immunity [4,5]. However, details of the pathophysiology of RA is not understood completely [6]. Local cytokines such as basic fibroblast growth factor (bFGF), platelet-derived growth factor (PDGF), transforming growth factor (TGF)-β, tumour necrosis factor (TNF)-α and IL-1β are considered to be responsible for the hyperplasia of FLS [7,8]. Upon activation, FLS produce TNF-α, IL-1β, IL-6 and matrix metalloproteinases, establishing the chronic and destructive inflammatory circuit [2]. The critical roles of these inflammatory cytokines have been shown by the effectiveness of cytokine-blockade therapies using anti-TNF-α or anti-IL-6 receptor antibodies for the treatment of RA [9,10]. However, it has also been recognized that certain RA subsets are resistant to these anti-cytokine therapies [11]. Such resistance may be explained partly by the intrinsic abnormality of RA-FLS independent of inflammation. Accumulated evidence has indicated that RA-FLS are stably activated and exhibit tumour-like characteristics. For example, they

destroyed human cartilage when they were transplanted together into severe combined immunodeficiency (SCID) mice [12]. RA-FLS expressed high levels of proto-oncogenes such as *c-myc* and *c-fos* [13,14]. In addition to these findings, RA-FLS are reported to express the tumour suppressor gene *TP53* with somatic mutations [15–19], and down-regulate the tumour suppressor *PTEN*, a protein phosphatase gene [20]. In particular, the somatic mutation of the *TP53* gene in RA-FLS appears consistent not only with their increased resistance to apoptosis but also with their proinflammatory properties such as the production of IL-6 and matrix metalloproteinase (MMP)-1 [21–23]. However, little is known about the mechanism by which the somatic mutations are introduced into the *TP53* gene in RA-FLS.

Activation-induced cytidine deaminase (AID) is a member of the APOBEC family, which is a cellular cytidine deaminase involved in protection from retrovirus infection or regulation of cholesterol metabolism [24]. AID was identified originally as an indispensable molecule for somatic hypermutation (SHM) at the immunoglobulin variable region and class-switch recombination in germinal centre B lymphocytes [25,26]. Recently, several papers have demonstrated that *AID* was up-regulated in non-lymphoid tumour cells such as breast cancer, cholangiocarcinoma, hepatoma and colorectal cancer cells [27–33]. Moreover, the somatic mutations of *TP53* found in these cancer cells appeared to be a direct target of AID [29,30].

In our study, we demonstrated that AID was expressed selectively by a fraction of RA-FLS, and that it was associated with somatic mutations in *TP53*. This suggests a possible mechanism by which the aberrant expression of AID within certain RA-FLS induces somatic mutations in *TP53*, leading to the acquisition of proinflammatory or tumour-like phenotypes.

Materials and methods

Cells and cell culture

Transformed human FLS cell lines were established from the synovial tissues of RA ($n = 9$; five males and four females) and osteoarthritis (OA) ($n = 9$; nine females) patients at the time of joint replacement surgery (Table 1). The tissues were obtained with the informed consent of the patients. Briefly, the synovial tissues were minced into small pieces and dissociated with collagenase and hyarulonidase in DMEM at 37°C for 1 h with shaking. After passing through mesh and washing with Dulbecco's modified Eagle's medium (DMEM), the synovial cells were suspended in the culture medium [DMEM containing 10% fetal calf serum (FCS) and penicillin/streptomycin] and plated in dishes. On the next day, non-adherent cells were removed and the medium was refreshed. The synovial cells were cultured in 10% CO_2 at 37°C with humidified air. After four passages, when it was ensured that no haematopoietic cells were present in the cell lines, plasmids pAct-SVT containing SV40T antigen were transduced with lipofectamine 2000 (Invitrogen, Carlsbad, CA, USA). All the cell lines showed fibroblast-like morphology and expressed CD44, CD106 and CD157/BST-1 on their surfaces, characteristic of synovial fibroblasts (data not shown). The transformed and original non-transformed primary FLS cells were maintained in DMEM supplemented with 10% heat-inactivated FCS with antibiotics. Materials for mRNA and protein analyses were obtained from the cell lines with passage numbers of <8 after thawing the frozen stocks. This study protocol was approved by the institutional review boards for ethics at the Faculty of Medicine, Osaka University (no. 340-1) and the Kawasaki Medical School (no. 291). For cell stimulation, FLS were cultured in phenol red-free DMEM (Sigma-Aldrich, St Louis, MO, USA) complete medium in the presence or absence of TNF-α (50 ng/ml; Pepro Tech Inc., Rocky Hill, NJ, USA), β-oestradiol (E_2; 10^{-9} M; Sigma-Aldrich) or both for 24 h.

Table 1. Characteristics of the patients in the study of transformed fibroblast-like synoviocytes.

	OA ($n = 9$)	RA ($n = 9$)
Age, mean (range) years	70·7 (64–80)	61·3 (35–75)
Sex, no. female/male	9/0	4/5
Disease duration, mean (range) years	n.a.	9·9 (4–19)
Medications, no. taking/no. assessed		
NSAIDs	9/9	6/9
DMARDs	0/9	7/9
Plus steroids	0/9	5/9
Soluble TNFR	0/9	1/9
No. RF+(>20IU)/no. assessed	n.a.	7/8
CRP, mean (range) mg/dl	n.a.	2·8 (0·7–5·3)
MMP-3, mean (range) ng/ml	n.a.	424·1 (49·7–973)

CRP, C-reactive protein; DMARDs, disease-modifying anti-rheumatic drugs; MMP, matrix metalloproteinase; n.a., not assessed; NSAID, non-steroidal anti-inflammatory drugs; OA, osteoarthritis; RF, rheumatoid factor; TNF, tumour necrosis factor.

Non-quantitative reverse transcription–polymerase chain reaction (RT–PCR) and quantitative real-time RT–PCR

Total RNAs were extracted using TRIzol® (Invitrogen), according to the manufacturer's instructions. Random hexamer-primed cDNAs were prepared using the ReverTra Ace® RT kit (Toyobo, Osaka, Japan) with 1 μg of total RNA and amplified by PCR using KOD-FX (Toyobo). The synthetic oligonucleotide primers for amplification of *AID*, *APOBEC1* and *APOBEC3G* were as follows: *AID*, 5′-AAATGTCCGCTGGGCTAAGG-3′ (forward) and 5′-GG AGGAAGAGCAATTCCACGT-3′ (reverse) [28]; *APOBEC1*, 5′-GGGACCTTGTTAACAGTGGAGT-3′ (forward) and 5′-CCAGGTGGGTAGTTGACAAAA-3′ (reverse); *APOBEC3G*,

5′-GAGCGCATGCACAATGAC-3′ (forward) and 5′-GCC TTCAAGGAAACCGTGT-3′ (reverse). The latter two primer sets were synthesized using Primer-BLAST (NCBI). The PCR for CD19 to exclude the contamination of B cells in FLS lines was conducted with the following primers: 5′-GACCTC ACCATGGCCCCTGG-3′ (forward) and 5′-CAGCCAG TGCCATAGTAC-3′ (reverse) [34]. The specific primers for human *AID* for quantitative real-time RT–PCR were designed using the Universal Primer Design Tools available on the Roche website. The 6-carboxyfluorescein-labelled probe for human *AID* was obtained from Roche (Universal Probe Library, probe no. 69; Roche Diagnostics, Indianapolis, IN, USA). The expression levels of target cDNAs were normalized to the endogenous transcription levels of human *GAPDH*. Gene expression was quantified using the 7500 real-time PCR system (PE Applied Biosystems, Foster City, CA, USA).

Western blot analysis

Whole-cell lysates (equivalent to 25 μg) in 1% TNE lysis buffer [1% Nonidet-P40, 150 mM NaCl, 10 mM Tris-HCl, pH 7·5, 1 mM ethylenediamine tetraacetic acid (EDTA)], in the presence of a protease inhibitor cocktail (Sigma-Aldrich) and protein kinase/phosphatase inhibitor cocktail (Roche) were subjected to Western blot analysis using polyvinylidine fluoride membrane and signal-enhancing kit (Santa Cruz Biotechnology Inc., Santa Cruz, CA, USA). The membrane was probed with rabbit anti-human AID antibody (Abcam, Cambridge, MA, USA) and reprobed with anti-β-actin antibody (Santa Cruz).

Immunocytochemistry and immunohistochemistry

We cultured 2×10^4 cells on the culture slide chamber (BD Falcon, Franklin Lakes, NJ, USA) for 12 h. After fixation with chilled acetone, the cells were washed and then blocked with 3% bovine serum albumin (BSA) in PBS. The cells were immunostained with either rabbit anti-human AID antibody (Abcam) combined with horseradish peroxidase-conjugated goat anti-rabbit immunoglobulin (Ig)G antibody (Southern Biotech, Birmingham, AL, USA) or with rat anti-human AID monoclonal antibody (mAb) (EK2 5G9; Cell Signaling Tech. Inc., Danvers, MA, USA) combined with biotinylated donkey anti-rat IgG antibody (Jackson ImmunoResearch Laboratories, Inc., West Grove, PA, USA) and vectastain elite ABC kit (Vector Laboratories Inc., Burlingame, CA, USA). The bound antibodies were visualized using diaminobenzidine (DAB) and counterstaining with haematoxylin. The images were obtained using a bright-field microscope (Axiophot, Carl Zeiss, Munich, Germany).

Cryosections with 6 μm thickness of the synovial tissues from RA patients were also stained with rat anti-human AID mAb after fixation with chilled acetone and detected as described above. The endogenous peroxidase activity was inactivated by treatment with 0·01% H_2O_2/PBS for 10 min at room temperature. Non-specific binding of second antibodies was blocked with PBS containing 5% of either normal goat or donkey serum for 30 min. To identify B cell follicles, mouse anti-human CD20 (Dako, Glostrup, Denmark) mAb and Envision goat anti-mouse and rabbit IgG antibody conjugated with horseradish peroxidase (Dako) were used. Rat anti-mouse CD4 mAb (GK1·5) was used as an isotype-matched control. For immunofluorescence staining, cryosections with 6 μm thickness of the synovial tissues from RA patients were fixed and stained with rat anti-human AID mAb and mouse anti-human CD20, the same as above. Either donkey anti-rat IgG antibody conjugated with Alexa 488 or donkey anti-mouse IgG antibody conjugated with Alexa 594 were used as second antibodies. Fluorescence images were obtained under the fluorescence microscope (Eclipse E800, Nikon, Tokyo, Japan).

Mutation analysis of TP53

The coding region of *TP53* spanning from exons 4–11 was amplified using high-fidelity DNA polymerase (iProof™, Bio-Rad, Hercules, CA, USA) with forward and reverse primers containing the *Sal*I and *Eco*RI sequences, respectively, as follows: forward, 5′-GCGTCGACCTACCAGGGC AGCTACGGTTTC-3′ and reverse, 5′-GGAATTCTTATGGC GGGAGGTAGACTGACC-3′. The amplicon was digested using restriction enzymes and subcloned into the corresponding cloning sites of the pBluescript vector. The insertion was sequenced with both the T3 and T7 primers located upstream and downstream of the cloning site, respectively, in pBluescript using sequence detector (Applied Biosystems). From the amplicons prepared from one FLS line, more than 35 colonies were picked up after bacterial transformation and each PCR product were sequenced. The sequence data were compared with those of the *TP53* nucleotide sequence obtained from GenBank (Accession number: NM_000546).

Results

Aberrant expression of AID in RA-FLS

First, we assessed the expression of the *AID* gene in transformed FLS cell lines obtained from OA and RA patients by RT–PCR. Surprisingly, *AID* was transcribed in more than half the RA-FLS lines (five of nine) and in none of the OA-FLS lines (Fig. 1a). In the RA-FLS lines *APOBEC1* was not expressed, whereas *APOBEC3G* was expressed ubiquitously, suggesting that *AID* transcription in RA-FLS is selective (Fig. 1a). Then, we used real-time PCR to quantify *AID* transcription among FLS. The same sets of RA-FLS showed approximately 7–18-fold higher *AID* transcription compared to the FLS from OA2 (Fig. 1b) that expressed a low but detectable level of AID transcription. Due probably to the higher sensitivity of probe-based real-time PCR, negligible

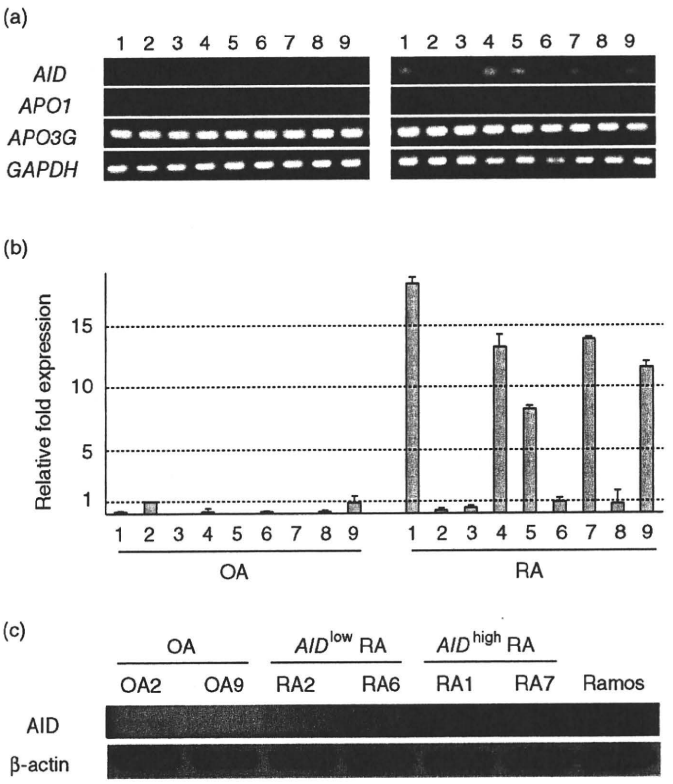

Fig. 1. Endogenous expression of activation-induced cytidine deaminase (AID) in rheumatoid arthritis-fibroblast-like synoviocytes (RA-FLS) lines. (a) The ectopic transcription of *AID* was detected in RA-FLS lines by reverse transcription–polymerase chain reaction (RT–PCR). The expression of two other APOBEC family members (*APO1*: APOBEC1, *APO3G*: APOBEC3G) was also examined by RT–PCR. (b) *AID* mRNA was quantified (relative quantification) by real-time PCR and normalized to housekeeping gene, *GAPDH* and fold expression over that of OA-FLS (OA2) was calculated by ΔΔCT method in triplicate. The grey bars and error bars indicate the averages and standard deviations, respectively, of two independent experiments. (c) Crude protein extracts from the representative FLS lines were analysed by sodium dodecyl sulphate-polyacrylamide gel electrophoresis (SDS-PAGE)/immunoblotting using anti-human AID polyclonal antibody (upper panel) or anti-β-actin (lower panel).

to very low levels of *AID* transcription were detectable by real-time PCR in the other four RA-FLS, as well as in some OA-FLS. Here, five RA-FLS with the expression levels of *AID* higher than fivefold compared with the level of OA2 are defined as AID^{high} FLS (RA1, 4, 5, 7, 9) and the other four RA-FLS (RA2, 3, 6, 8) with the equivalent levels to OA-FLS are defined as AID^{low} FLS. This aberrant expression of *AID* is not likely to have resulted by contamination of B cells expressing *AID*, because the synovial cell culture was occupied with adherent and morphologically fibroblast-like cells after four passages. The possibility of B cell contamination was clearly excluded because no transcription of CD19, a pan B cell marker, was detectable in the AID^{high} FLS (data not shown, but the primer pairs are described in Materials and methods). Next, we confirmed the endogenous expression of the AID protein by Western blot analysis with the two representative cell lines from OA, AID^{low} RA and AID^{high} RA (Fig. 1c).

The aberrant expression of AID in a fraction of RA-FLS prompted us to investigate its correlation with the clinical characteristics in nine RA patients from whom FLS were established. The frequencies of AID^{high} RA-FLS were 75% (three of four) and 40% (two of five) in RA-FLS derived from female and male RA patients, respectively. No correlation was observed in the ages, serum MMP-3 levels or medicines prescribed to the patients. Laboratory data revealed the tendency of higher C-reactive protein (CRP) levels in the AID^{high} RA-FLS than in the AID^{low} RA-FLS (3·9 ± 1·7 *versus* 1·5 ± 0·6, respectively), although the sample size of our study is too small to detect these correlations adequately. These data suggested that AID expression in FLS might be facilitated under conditions of inflammation in female patients. Because inflammatory cytokines and oestrogen have been reported to induce *AID* transcription [28,30,35], we investigated whether this is also the case in FLS. In OA-FLS with low levels of *AID* expression, TNF-α but not physiological concentration of β-oestradiol (E_2) augmented the transcription of *AID*, and simultaneous stimulation with E_2 and TNF-α exhibited synergistic effects (Fig. 2). In AID^{low} RA-FLS, E2 or TNF-α alone enhanced the transcription of *AID* much higher than OA-FLS, although the synergistic effect was not obvious. Even in AID^{high} RA-FLS, E_2 or TNF-α alone augmented the transcription of *AID*, which resulted in more than 20-fold higher levels of *AID* transcription compared with basal levels those in OA-FLS. It is of note that physiological concentration of β-oestradiol up-regulated *AID* transcription only in RA-FLS, suggesting intrinsic RA-FLS abnormality in the susceptibility of *AID* induction to female sex steroids. As another molecular mechanism for *AID* induction, negative regulatory roles for the microRNA miR-155 on AID transcription have been reported in previous studies on germinal centre B cells [36,37], but there was no significant down-regulation of miR-155 in AID^{high} RA-FLS (data not shown). Real-time PCR analyses of RA-FLS did not show *TNF-α* transcription or correlation between the transcription levels of *IL-6* or *IL-1β*

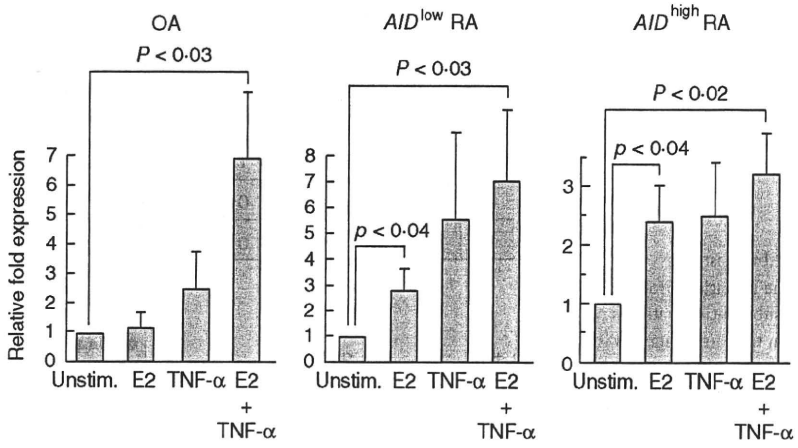

Fig. 2. Inducible expression of *AID* in transformed fibroblast-like synoviocytes (FLS) lines by stimulation with tumour necrosis factor (TNF)-α and oestrogen. One million osteoarthritis (OA)-FLS (OA2, OA6 and OA9), *AID*^{low} RA-FLS (RA2, RA3 and RA6) and *AID*^{high} RA-FLS (RA1, RA4 and RA7) were stimulated in phenol red-free Dulbecco's modified Eagle's complete medium (DMEM) with either TNF-α (50 ng/ml) or β-oestradiol (E_2; 10^{-9} M) for 24 h. The *AID* transcription was quantified (relative quantification) by real-time polymerase chain reaction (PCR) and normalized to the housekeeping gene, *GAPDH* and the relative fold induction over the unstimulated cells (Unstim.) was monitored by the ΔΔCT method. The grey bars and error bars indicate the averages and standard deviations, respectively, of three cell lines. *P*-values calculated by Student's *t*-test are indicated.

with that of *AID* (data not shown), suggesting that *AID* transcription is induced passively by external stimuli present most commonly in RA rather than that provided by inflammatory cytokines in an autocrine fashion.

Accumulation of *TP53* gene mutations in AID-expressing RA-FLS

Detailed studies have established that the mutations of the p53 tumour suppressor gene found in RA-FLS could contribute to both the tumour-like and proinflammatory properties of RA-FLS, such as aggressive growth, invasion and destruction of cartilage and bone [15–19,21–23]. Although genotoxic and oxidative stresses have been speculated to be the causative candidates for the somatic mutation in the *TP53* gene in RA-FLS, the molecular mechanism has not yet been elucidated. Recently, a clear relationship between AID expression and the frequency of *TP53* somatic mutations has been demonstrated in some non-B lymphocytes, such as hepatocytes and colon epithelial cells [29–33]. To investigate whether this is the case for RA-FLS, the coding region of *TP53* was amplified by RT–PCR with high-fidelity polymerase, sequenced and then compared among OA-FLS, *AID*^{low} RA-FLS and *AID*^{high} RA-FLS. The frequency of *TP53* somatic mutations was elevated significantly in *AID*^{high} RA-FLS rather than in OA-FLS and *AID*^{low} RA-FLS (summarized in Table 2). Although sporadic mutations were detected even in the latter two FLS, *AID*^{high} RA-FLS exhibited approximately two- to 3·5-fold more mutations than the other two FLS subsets. In addition, the frequency of non-

Table 2. Mutation frequency of TP53.

	Number of base substitution	Total base pair of sequenced	Frequency/10 000	Mutation		
				Silent	Missense	Non-sense
OA2	0	23 587	0	0	0	0
OA6	0	25 150	0	0	0	0
OA9	1	27 146	0·368	1	0	0
RA2	2	22 456	0·891	2	0	0
RA3	1	29 459	0·339	0	1	0
RA6	2	24 631	0·812	1	1	0
RA1	8	26 187	3·054	2	6	0
RA4	6	26 655	2·251	2	4	0
RA7	4	23 657	1·691	0	3	1

cDNA was prepared from representative fibroblast-like synoviocyte (FLS) lines in each group. Osteoarthritis (OA)-FLS: OA2, OA6 and OA9. Activation-induced cytidine deaminase (AID)^{low} rheumatoid arthritis (RA)-FLS: RA2, RA3 and RA6. AID^{high} RA-FLS: RA1, RA4 and RA7. The coding region of *TP53* ranging from exons 4–11 was amplified using high-fidelity DNA polymerase. Mutation frequency was analysed by sequencing of polymerase chain reaction product.

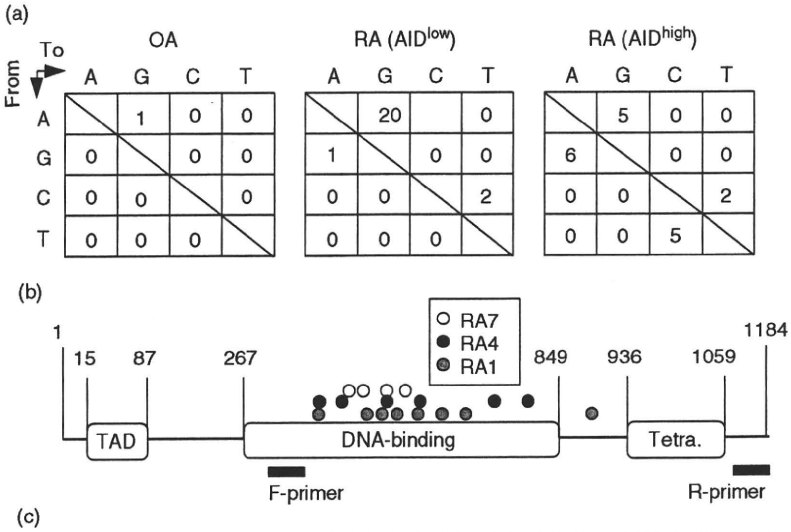

(c)

RA1 Base change	Amino acid at mutation site	RA4 Base change	Amino acid at mutation site	RA7 Base change	Amino acid at mutation site
770 (T→C)	L257P	412 (G→A)	A138T	516 (T→C)	V172A
713 (G→A)	C238Y	606 (T→C)	R202R	505 (A→G)	M169V
483 (C→T)	A161A	459 (C→T)	P153P	443 (A→G)	D148G
367 (A→G)	T123A	544 (T→C)	C182R	438 (G→A)	W146STOP
914 (A→G)	K305R	805 (A→G)	S269G		
500 (G→A)	Q305R	743 (G→A)	R248Q		
666 (G→A)	Q167R				
679 (T→C)	P222P				
	S227P				

Fig. 3. *TP53* mutations in fibroblast-like synoviocytes (FLS). (a) Gene mutation profiles of *TP53* in FLS lines. Base substitution patterns seen in *TP53* extracted from the same data sets as those used for the mutation frequency analysis in Table 1 are shown. The numbers in the box are the sum of three FLS lines in each group. (b) Distribution of gene mutations in *TP53* from FLS lines. Each number in the figure corresponds to the position of nucleotide on the coding sequence of *TP53*. Open circles are from RA7, filled circles are from RA4 and grey circles are from RA1. The location of polymerase chain reaction (PCR) primers used for sequencing is also depicted. TAD: transactivation domain; Tetra. tetramerization domain. (c) Base and amino acids substitution in *TP53* from three of *AID*^{high} RA-FLS lines. Amino acids are described in a single letter. The two shaded mutations in RA1 were double mutations found in one clone.

silent mutations was three times greater than that of silent mutations. Notably, the dominant base substitution pattern is the transition type, which is very similar to the mutations found at the variable region of the immunoglobulin gene, introduced exclusively by AID (Fig. 3a) [26]. Introduction of somatic mutations at the Ig variable region by AID is coupled with the transcription level of the *Ig* gene [38] because AID attacks the single-strand DNA that appears at transcription. Thus, the somatic mutation requires both the expression of AID and the transcription of the target gene. Among the representative FLS lines, *TP53* was transcribed constitutively and the amounts of *TP53* mRNA were comparable, indicating that the increased frequency of mutation in *TP53* resulted mainly from *AID* expression rather than the transcription levels of *TP53* (data not shown). Compared with *TP53* mutations in previous reports [15,18,19,22], 17% of the mutations that we identified resulted in the changes of amino acids identical with those and 33% of those in different amino acids, but were located at the same codon. The non-sense mutation in RA7 in this study occurred at the same position as that reported by Yamanishi *et al.* [22].

While the sequencing range did not cover the whole coding sequence of *TP53*, the mutations in the *TP53* gene were obviously concentrated at the DNA-binding domain, which is the hotspot of somatic mutations found in some malignant tumours (Fig. 3b). In particular, the Arg^{248} mutation found in RA4 has been reported as one of the cancer hotspot mutations [39]. The details of both base and amino acid substitutions are listed in Fig. 3c. These data indicate that *AID*^{high} RA-FLS have higher frequencies of *TP53* mutations, some of which could result in the loss of function of TP53.

AID is expressed by non-transformed RA-FLS and in the RA-synovium outside of the B cell follicles

To address the issue of whether the aberrant expression of AID is affected by the transformation with SV40 large T antigen, first we examined the endogenous AID expression in non-transformed primary cell lines of FLS. *AID* transcription was detectable in four of 11 primary RA-FLS at three to eight times higher levels compared to transformed OA-FLS, but in none of six primary OA-FLS (Fig. 4a, and data not shown), indicating that increased expression of *AID* in RA-FLS is independent of transformation with SV40 large T antigen.

We then examined the production of AID protein in non-transformed RA-FLS. Cytostaining with two different anti-AID antibodies clearly exhibited the production of AID protein in *AID*$^+$ primary RA-FLS (Fig. 4b, i and ii corresponding to pRA5) but not in *AID*$^-$ primary OA-FLS (Fig. 4b, iii and iv, corresponding to pOA9). These data dem-

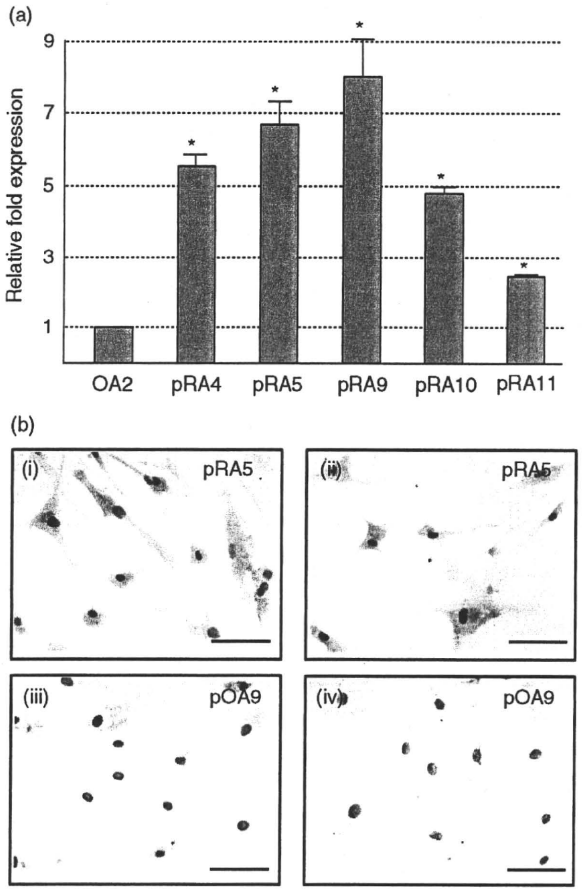

Fig. 4. Endogenous expression of activation-induced cytidine deaminase (AID) in non-transformed primary rheumatoid arthritis-fibroblast-like synoviocytes (RA-FLS). The identical number of primary FLS corresponding to that of transformed FLS indicates that both are derived from the same patient, except for pRA10 and pRA11, which have no corresponding transformants. (a) The expression level of *AID* was estimated and compared between transformed osteoarthritis (OA2) as control and non-transformed primary RA-FLS by real-time polymerase chain reaction (PCR). Relative fold expression was determined by the *AID* expression in OA2 being defined as 1. The grey bars and error bars indicate the averages and standard deviations, respectively, of two independent experiments. Asterisks indicate the statistically significant difference by Student's *t*-test. *P*-value < 0·01. Uncapitalized *p* at the head of RA means 'primary'. (b) Primary FLS grown on the glass slide were stained with rabbit anti-AID polyclonal antibody used in Western blot analysis (i and iii) or rat anti-AID monoclonal antibody (mAb) (ii and iv) combined with horseradish peroxidase-conjugated second antibodies. Diaminobenzidine was used as chromogenic substrate. Primary FLS cells from the same source of RA5 (i and ii, pRA5) and of OA9 (iii and iv, pOA9) are shown. Nuclear staining was performed with haematoxylin (violet). Scale bar indicates 100 μm.

onstrated clearly that the ectopic production of AID in RA-FLS is not a secondary effect by SV40 transformation.

Next, to examine whether AID production by RA-FLS is not the artefact *in vitro*, but the real event in the RA synovium *in situ*, we conducted immunohistochemical staining on the serial sections of the synovium from AID$^+$ RA patients with anti-CD20, anti-AID and control antibodies. The localization of CD20$^+$ B cells clearly isolated the follicles in the synovium (Fig. 5a, d), with a low frequency of AID-positive B cells. However, the majority of cells reacted by anti-AID antibody localized clearly in the lining and sublining outside the follicles (Fig. 5b, e). Isotype-matched irrelevant antibody towards mouse CD4 showed no signal on the serial specimen (Fig. 5c, f). Larger magnification revealed that AID signals were raised mainly from CD20$^-$ non-B cells that are morphologically compatible with FLS (Fig. 5g, h, black arrows), and some signals are originated from CD20$^+$ B cells (Fig. 5g, h, red arrows). To ensure this finding, double immunofluorescence staining with anti-AID and -CD20 mAbs was performed. The reactivity of anti-AID mAb (green) was obvious only in the AID-positive synovial tissue (Fig. 6a, c) but not in the AID-negative tissue (Fig. 6b, d). In higher magnification (Fig. 6e), the distinct area consisting of the cells reactive only to anti-AID mAb (green) spread well outside the area containing CD20$^+$ cells (red). The cells expressing both molecules are yellow and marked with an arrowhead in the figure.

These results demonstrated clearly that the FLS in the RA synovial tissues produce AID, providing strong evidence that ectopic and aberrant expression of AID occurs in RA.

Discussion

We have demonstrated that AID is expressed preferentially in transformed FLS cell lines from RA patients and that *AID* expression was correlated with accumulation of mutations in p53 gene. TNF-α enhanced the transcription of *AID* in both RA- and OA-FLS, whereas physiological concentration of β-oestradiol enhanced it only in RA-FLS. The selective and enhanced expression of *AID* was also confirmed in primary, non-transformed RA-FLS. Furthermore, localization of AID production outside the B cell follicles was demonstrated in the RA synovium tissue, providing definitive evidence that *AID* is expressed aberrantly and ectopically in certain cases of RA synovium. Thus, AID is a novel and intriguing candidate for the cause of the p53 mutation that has been reported to contribute the tumour-like phenotypes of RA-FLS.

To see the effects of *TP53* mutations on SV40-transformed RA-FLS, we examined the cell number after 4 days' culture and the transcription levels of *IL-6* and *MMP-1* by real-time PCR analysis, both of which did not demonstrate any correlation with expression of *AID*. Despite the concomitant detection of *TP53* mutations with *AID* transcription in a fraction of RA-FLS, the cell lines did not exhibit any tumour-

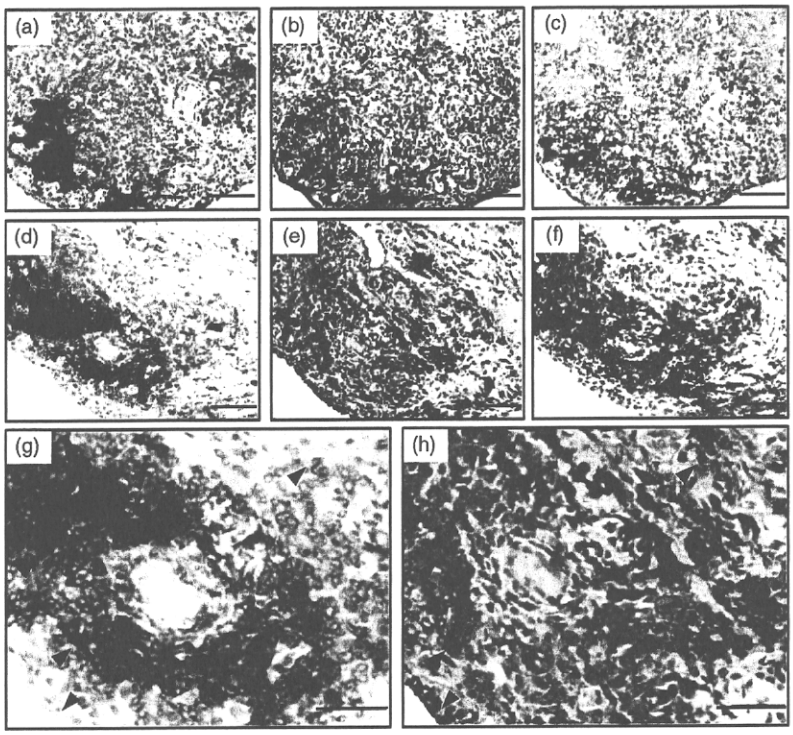

Fig. 5. Immunohistochemical studies of activation-induced cytidine deaminase (AID) expression on synovial tissue section from the representative rheumatoid arthritis (RA) patient. The (a) (d) and (g) sections were stained with anti-CD20 monoclonal antibody (mAb) to identify the location of the B cell-containing follicle in synovial tissue. The (b) (e) and (h) sections were with the rat mAb for AID, and (c) and (f) were with isotype-matched control antibody. The serial sections of (a) (b) and (c) were from RA4, and of (d) (e) and (f) were from RA5. The (g) and (h) sections were high-power fields corresponding to (d) and (e), respectively. Red and black arrows indicate B cells and non-B cells, respectively. Nuclear staining was performed with haematoxylin (violet). Scale bar indicates 100 μm.

like growth advantages or proinflammatory characteristics. However, this is plausible, because our sequence analyses could detect the generation of *TP53* mutations in the very low-frequent clones that are not sufficiently predominant to affect the characteristics of the AID^{high} RA-FLS line as a whole. Although not definitive, there was an informative and supportive RA case from which we obtained the two FLS lines from different joint lesions at distinct times of operation with a 6-month interval. Interestingly, AID expression was detectable only in the cell line established after the second operation, suggesting the possibility that ectopic expression of AID was acquired during the course of RA (unpublished observation). These intriguing possibilities should be tested using a larger sample size of clinical cases and/or quantitative histological analyses.

Xu *et al.* reported that B cells in the follicle of synovium or in the peripheral blood from RA patients show a higher expression level of AID in comparison with OA patients

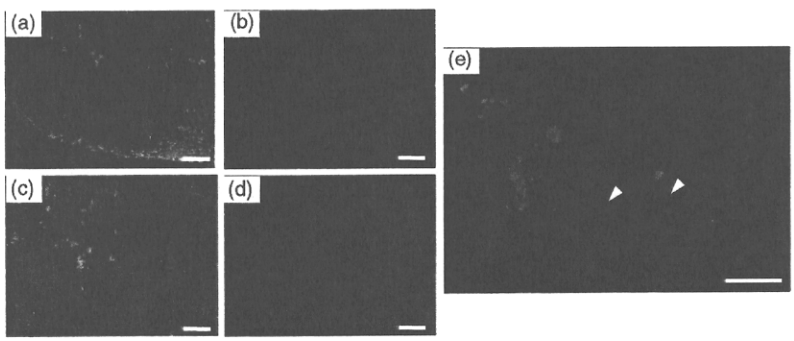

Fig. 6. Immunofluorescence staining of activation-induced cytidine deaminase (AID) on synovial tissue sections from the representative rheumatoid arthritis (RA) patient. All sections were stained with rat monoclonal antibody (mAb) for AID and anti-CD20 mAb simultaneously. AID was visualized with Alexa 488 fluoro-dye-conjugated anti-rat secondary antibody (green) and CD20 was visualized with Alexa 594 fluoro-dye-conjugated anti-mouse secondary antibody (red) and observed under fluoresence microscope. The sections of (a) were from an AID-positive RA sample corresponding to RA4, and of (b) was from another AID-negative RA sample from which no transformed cell line had been established. The sections of (c) and (e) were high-power fields corresponding to (a), and (d) were high-power fields corresponding to (b). White arrowheads indicate the cells expressing both AID and CD20. Nuclear staining was performed with 4,6-diamidino-2-phenylindole (violet). Scale bar indicates 100 μm in (a) and (b), 50 μm in (c) (d) and (e).

[40]. Our analyses in this paper demonstrated selective expression of AID in both transformed and non-transformed FLS from RA. Furthermore, immunohistochemical analysis of our RA cases revealed that major AID-producing cells with FLS-like morphology localized in the area outside B cell follicles; B cell follicles without production of AID were also described by them. When these results by us and others are integrated, we hypothesize that both B cells and non-B cells in RA patients are liable to express AID as an intrinsic or secondary abnormality under inflammatory milieu, which is responsible for the various aspects in the pathophysiology of RA. Higher expression of AID in B cells causes the SHM at variable regions in *Ig* gene and involvement in the generation of autoreactive B cells, which produce autoantibodies such as RF and anti-CCP antibody. Conversely, ectopic expression of AID in non-B cells, such as FLS *per se*, introduces point mutations in some genes, including tumour suppressor genes, and alters the phenotype of the cells including FLS.

It may be imagined that AID could be a potential therapeutic target for RA; however, it would be difficult to know when AID expression has begun in FLS in the synovium of each RA case. Although we did not study in detail the triggers for the ectopic expression of *AID* in FLS of RA, it is reasonable to speculate that anti-inflammatory cytokine therapy starting at earlier stages of RA suppresses the induction of AID expression in FLS and might prevent the malignant transformation of FLS by AID-dependent random mutagenesis.

Acknowledgements

We thank Ms Reina Tanaka for her technical assistance. We also thank Dr Kazuhiko Kuwahara at Kumamoto University for providing us with the SW480 colorectal cancer cell line, which was used for the positive control on APOBEC1 amplification. This work was supported by Research Project Grants (20-418I to H.I. and 19-406M to K.I.) from Kawasaki Medical School and Grants-in-Aid for Scientific Research from the Ministry of Education, Science, Sports, Culture and Technology of Japan (19590390 to K.I.).

Disclosure

None.

References

1 Lipsky PE. Rheumatoid arthritis. In: Fauci AS, Braunwald E, Kasper DL *et al.*, eds. Harrison's principles of internal medicine, 17th edn. New York: McGraw-Hill Professional, 2008:2083–91.
2 Firestein GS. Evolving concepts of rheumatoid arthritis. Nature 2003; **423**:356–61.
3 Mor A, Abramson SB, Pillinger MH. The fibroblast-like synovial cell in rheumatoid arthritis: a key player in inflammation and joint destruction. Clin Immunol 2005; **115**:118–28.
4 Kirkham BW, Lassere MN, Edmonds JP *et al.* Synovial membrane cytokine expression is predictive of joint damage progression in rheumatoid arthritis: a two-year prospective study (the damage study cohort). Arthritis Rheum 2006; **54**:1122–31.
5 Miossec P, Korn T, Kuchroo VK. Interleukin-17 and type 17 helper t cells. N Engl J Med 2009; **361**:888–98.
6 Andersson AK, Li C, Brennan FM. Recent developments in the immunobiology of rheumatoid arthritis. Arthritis Res Ther 2008; **10**:204.
7 Feldmann M, Brennan FM, Maini RN. Role of cytokines in rheumatoid arthritis. Annu Rev Immunol 1996; **14**:397–440.
8 McInnes IB, Schett G. Cytokines in the pathogenesis of rheumatoid arthritis. Nat Rev Immunol 2007; **7**:429–42.
9 Nishimoto N, Kishimoto T. Interleukin 6: from bench to bedside. Nat Clin Pract Rheumatol 2006; **2**:619–26.
10 Brennan FM, McInnes IB. Evidence that cytokines play a role in rheumatoid arthritis. J Clin Invest 2008; **118**:3537–45.
11 Firestein GS. Biomedicine. Every joint has a silver lining. Science 2007; **315**:952–3.
12 Pierer M, Muller-Ladner U, Pap T, Neidhart M, Gay RE, Gay S. The SCID mouse model: novel therapeutic targets – lessons from gene transfer. Springer Semin Immunopathol 2003; **25**:65–78.
13 Roivainen A, Pirila L, Yli-Jama T, Laaksonen H, Toivanen P. Expression of the myc-family proto-oncogenes and related genes max and mad in synovial tissue. Scand J Rheumatol 1999; **28**:314–18.
14 Aikawa Y, Morimoto K, Yamamoto T *et al.* Treatment of arthritis with a selective inhibitor of c-fos/activator protein-1. Nat Biotechnol 2008; **26**:817–23.
15 Firestein GS, Echeverri F, Yeo M, Zvaifler NJ, Green DR. Somatic mutations in the p53 tumor suppressor gene in rheumatoid arthritis synovium. Proc Natl Acad Sci USA 1997; **94**:10895–900.
16 Reme T, Travaglio A, Gueydon E, Adla L, Jorgensen C, Sany J. Mutations of the p53 tumour suppressor gene in erosive rheumatoid synovial tissue. Clin Exp Immunol 1998; **111**:353–8.
17 Kullmann F, Judex M, Neudecker I *et al.* Analysis of the p53 tumor suppressor gene in rheumatoid arthritis synovial fibroblasts. Arthritis Rheum 1999; **42**:1594–600.
18 Inazuka M, Tahira T, Horiuchi T *et al.* Analysis of p53 tumour suppressor gene somatic mutations in rheumatoid arthritis synovium. Rheumatology (Oxf) 2000; **39**:262–6.
19 Yamanishi Y, Boyle DL, Green DR *et al.* P53 tumor suppressor gene mutations in fibroblast-like synoviocytes from erosion synovium and non-erosion synovium in rheumatoid arthritis. Arthritis Res Ther 2005; **7**:R12–R18.
20 Pap T, Franz JK, Hummel KM, Jeisy E, Gay R, Gay S. Activation of synovial fibroblasts in rheumatoid arthritis: lack of expression of the tumour suppressor pten at sites of invasive growth and destruction. Arthritis Res 2000; **2**:59–64.
21 Han Z, Boyle DL, Shi Y, Green DR, Firestein GS. Dominant-negative p53 mutations in rheumatoid arthritis. Arthritis Rheum 1999; **42**:1088–92.
22 Yamanishi Y, Boyle DL, Rosengren S, Green DR, Zvaifler NJ, Firestein GS. Regional analysis of p53 mutations in rheumatoid arthritis synovium. Proc Natl Acad Sci USA 2002; **99**:10025–30.
23 Sun Y, Zeng XR, Wenger L, Firestein GS, Cheung HS. P53 down-regulates matrix metalloproteinase-1 by targeting the

communications between ap-1 and the basal transcription complex. J Cell Biochem 2004; **92**:258–69.

24 Goila-Gaur R, Strebel K. Hiv-1 vif, apobec, and intrinsic immunity. Retrovirology 2008; **5**:51.

25 Honjo T, Muramatsu M, Fagarasan S. Aid: how does it aid antibody diversity? Immunity 2004; **20**:659–68.

26 Di Noia JM, Neuberger MS. Molecular mechanisms of antibody somatic hypermutation. Annu Rev Biochem 2007; **76**:1–22.

27 Babbage G, Ottensmeier CH, Blaydes J, Stevenson FK, Sahota SS. Immunoglobulin heavy chain locus events and expression of activation-induced cytidine deaminase in epithelial breast cancer cell lines. Cancer Res 2006; **66**:3996–4000.

28 Endo Y, Marusawa H, Kinoshita K *et al.* Expression of activation-induced cytidine deaminase in human hepatocytes via nf-kappab signaling. Oncogene 2007; **26**:5587–95.

29 Kou T, Marusawa H, Kinoshita K *et al.* Expression of activation-induced cytidine deaminase in human hepatocytes during hepatocarcinogenesis. Int J Cancer 2007; **120**:469–76.

30 Endo Y, Marusawa H, Kou T *et al.* Activation-induced cytidine deaminase links between inflammation and the development of colitis-associated colorectal cancers. Gastroenterology 2008; **135**:889–98, 98 e1-3.

31 Komori J, Marusawa H, Machimoto T *et al.* Activation-induced cytidine deaminase links bile duct inflammation to human cholangiocarcinoma. Hepatology 2008; **47**:888–96.

32 Morisawa T, Marusawa H, Ueda Y *et al.* Organ-specific profiles of genetic changes in cancers caused by activation-induced cytidine deaminase expression. Int J Cancer 2008; **123**:2735–40.

33 Chan-On W, Kuwahara K, Kobayashi N *et al.* Cholangiocarcinomas associated with long-term inflammation express the activation-induced cytidine deaminase and germinal center-associated nuclear protein involved in immunoglobulin v-region diversification. Int J Oncol 2009; **35**:287–95.

34 Szczepek AJ, Bergsagel PL, Axelsson L, Brown CB, Belch AR, Pilarski LM. CD34+ cells in the blood of patients with multiple myeloma express CD19 and igh mrna and have patient-specific igh vdj gene rearrangements. Blood 1997; **89**:1824–33.

35 Pauklin S, Sernandez IV, Bachmann G, Ramiro AR, Petersen-Mahrt SK. Estrogen directly activates aid transcription and function. J Exp Med 2009; **206**:99–111.

36 Dorsett Y, McBride KM, Jankovic M *et al.* Microrna-155 suppresses activation-induced cytidine deaminase-mediated myc-igh translocation. Immunity 2008; **28**:630–8.

37 Teng G, Hakimpour P, Landgraf P *et al.* Microrna-155 is a negative regulator of activation-induced cytidine deaminase. Immunity 2008; **28**:621–9.

38 Shen HM, Poirier MG, Allen MJ *et al.* The activation-induced cytidine deaminase (aid) efficiently targets DNA in nucleosomes but only during transcription. J Exp Med 2009; **206**:1057–71.

39 Ko LJ, Prives C. P53: puzzle and paradigm. Genes Dev 1996; **10**:1054–72.

40 Xu X, Hsu HC, Chen J *et al.* Increased expression of activation-induced cytidine deaminase is associated with anti-ccp and rheumatoid factor in rheumatoid arthritis. Scand J Immunol 2009; **70**:309–16.

Mod Rheumatol (2011) 21:10–15
DOI 10.1007/s10165-010-0325-3

ORIGINAL ARTICLE

Humanized anti-interleukin-6-receptor antibody (tocilizumab) monotherapy is more effective in slowing radiographic progression in patients with rheumatoid arthritis at high baseline risk for structural damage evaluated with levels of biomarkers, radiography, and BMI: data from the SAMURAI study

Jun Hashimoto · Patrick Garnero · Désirée van der Heijde · Nobuyuki Miyasaka · Kazuhiko Yamamoto · Shinichi Kawai · Tsutomu Takeuchi · Hideki Yoshikawa · Norihiro Nishimoto

Received: 3 March 2010 / Accepted: 31 May 2010 / Published online: 24 June 2010

Abstract Our aim was to assess the ability of tocilizumab monotherapy to reduce progressive structural joint damage in rheumatoid arthritis patients at high risk of progression. This study was a subanalysis from a prospective 1-year, multicenter, X-ray-reader-blinded, randomized controlled trial of tocilizumab [Study of Active Controlled Monotherapy Used for Rheumatoid Arthritis, an IL-6 Inhibitor (SAMURAI) trial]. All patients were categorized into two or three groups according to four independent predictive markers for progressive joint damage [urinary C-terminal crosslinking telopeptide (uCTX-II), urinary pyridinoline/deoxypyridinoline (uPYD/DPD) ratio, body mass index (BMI), and joint-space narrowing (JSN) score at baseline]. One-year progression of joint destruction was assessed in high-risk versus low-risk groups receiving tocilizumab monotherapy and compared with patients receiving conventional disease-modifying antirheumatic drugs (DMARDs) ($n = 157$ and 145, respectively). In patients at high risk of progression of erosion as estimated by high uCTX-II, uPYD/DPD, or low BMI, and at high risk of progression of JSN as estimated by low BMI or high JSN score, the 52-week changes in radiological erosion and JSN, respectively, were significantly less in patients treated with tocilizumab monotherapy compared with those receiving DMARDs for each type of risk factor. In patients at low risk, those receiving tocilizumab also progressed less than those on DMARDs, although the difference did not reach statistical significance. Tocilizumab monotherapy is more effective in reducing radiological progression in patients presenting with risk factors for rapid progression than in low-risk patients. Patients at high risk for progression may benefit more from tocilizumab treatment.

Keywords CTX-II · PYD/DPD · Rheumatoid arthritis · Interleukin-6 · Tocilizumab · Joint destruction

J. Hashimoto · H. Yoshikawa
Osaka University Graduate School of Medicine, Osaka, Japan

P. Garnero
INSERM Research Unit 664, Lyon, France

D. van der Heijde
University Hospital Maastricht, Maastricht, The Netherlands

N. Miyasaka
Tokyo Medical and Dental University, Tokyo, Japan

K. Yamamoto
The University of Tokyo, Tokyo, Japan

S. Kawai
Toho University, Tokyo, Japan

T. Takeuchi
Keio University, Tokyo, Japan

N. Nishimoto
Wakayama Medical University, Wakayama, Japan

N. Nishimoto (✉)
Laboratory of Immune Regulation,
Wakayama Medical University, 105 Saito Bio Innovation Center, 7-7-20 Saito-Asagi, Ibaraki, Osaka 567-0085, Japan
e-mail: norichan@wakayama-med.ac.jp

Introduction

Biological agents targeting inflammatory cytokines have proven more effective than conventional disease-modifying antirheumatic drugs (DMARDs) for suppressing disease activity and progressive joint damage in rheumatoid arthritis (RA) [1–11]. Patients at high risk of progressive joint damage who are difficult to treat with conventional

DMARDs may be a particularly important target population for treatment with biologics. Our recent studies showed that increased urinary levels of C-terminal cross-linked telopeptide of type II collagen (uCTX-II), total pyridinoline/total deoxypyridinoline ratio (uPYD/DPD ratio), joint-space narrowing (JSN) score, and low body mass index (BMI) at baseline were all independent predictive markers for radiographically evident joint damage in patients with RA of <5 years and treated with conventional DMARDs. Although targeting patients with rapid progression, as assessed by these predictive factors, for treatment with biologics may be beneficial, to date there is no evidence that these agents are equally effective in such high-risk patients. Therefore, this study aimed to investigate the ability of tocilizumab monotherapy to reduce progressive structural joint damage in high-risk patients.

Methods

Patients with RA of <5 year duration participating in a prospective 1-year randomized controlled trial of tocilizumab [Study of Active Controlled Monotherapy Used for Rheumatoid Arthritis, an IL-6 Inhibitor (SAMURAI) trial] [10] receiving anti-interleukin (IL)-6-receptor antibody monotherapy (8 mg/kg intravenously every 4 weeks, $n = 154$), were categorized into two or three groups according to their uCTX-II values, uPYD/DPD ratio, BMI, and JSN scores at baseline (cutoff values: 500 ng/mmol creatinine for uCTX-II, median for uPYD/DPD, 0 units for JSN, 18.5 and 25 for BMI). These four factors were shown to be independent predictive markers for radiographically evident joint damage progression in 148 patients with RA treated with conventional DMARDs in the control arm of the SAMURAI trial [12]. Briefly, this trial established that high baseline uCTX-II, uPYD/DPD ratio and JSN score and a low BMI were independent risk factors for progression of bone erosion as evaluated with the van der Heijde modified Sharp method in patients with RA receiving conventional DMARDs. In addition to these three variables, the JSN score at baseline was also significantly associated with an increased risk of progression of JSN score and total Sharp score (TSS). In this study, we compared the 1-year progression of joint destruction in these high- and low-risk groups in the two cohorts of 148 and 154 patients with RA receiving conventional DMARDs or tocilizumab monotherapy, respectively.

SAMURAI trial

In the SAMURAI trial [10], patients were >20 years and fulfilled the American College of Rheumatology (ACR; formerly the American Rheumatism Association) 1987 revised criteria for the classification of RA, with a disease duration of ≥6 months and <5 years. In addition, they had ≥6 tender joints (of 49 evaluated), ≥6 swollen joints (of 46 evaluated), an erythrocyte sedimentation rate (ESR) of ≥30 mm/h, and C-reactive protein (CRP) of ≥20 mg/l. All patients had an inadequate response to at least one DMARD or immunosuppressant. Use of anti-tumor necrosis factor (anti-TNF) agents and leflunomide were not allowed within the 3 months prior to the first dose. Change in dose and type of DMARDs and/or immunosuppressants, plasma exchange therapies, and surgical treatments were not allowed within the previous 4 weeks. Oral corticosteroids (prednisolone up to 10 mg/day) were allowed if the dosage had not been changed during the prior 2 weeks. Patients were randomly assigned to receive either tocilizumab monotherapy at 8 mg/kg intravenously every 4 weeks or conventional DMARD therapy for 52 weeks. For the tocilizumab group, DMARDs and/or immunosuppressants were discontinued from the start of the study. Oral corticosteroids (up to 10 mg prednisolone per day) were allowed, but the dosage could not be increased during the study. Use of one nonsteroidal anti-inflammatory drug (NSAID), including switching to another NSAID, was allowed. For the conventional DMARD group, the dose, type, and combination of DMARDs and/or immunosuppressants, except for anti-TNF agents and leflunomide, could be varied according to disease activity at the discretion of the treating physician. Variations of NSAIDs and/or corticosteroids including intra-articular corticosteroid injections were also allowed.

Assessment of risk of radiographic progression

Posteroanterior radiographs of the hands and anteroposterior radiographs of the feet were acquired at baseline, week 28, and week 52 (or at the last visit for patients who withdrew from the study prior to week 52). Radiographs were scored using the van der Heijde modified Sharp method [13] for bone erosion, JSN, and TSS independently by two readers who were well trained and competent to score radiographs in accordance with the method. The readers were blinded to the treatment group and chronologic order of the images. We measured urinary total deoxypyridinoline (uDPD) and total pyridinoline (uPYD) by high-performance liquid chromatography (HPLC) and uCTX-II by enzyme-linked immunosorbent assay (ELISA) (CTX-II CartiLaps® ELISA, NORDIC Biosciences, Herlev, Denmark).

Statistical analysis

All statistical analyses were two-sided, and p values <0.05 were considered significant. All statistical analyses were carried out using SAS (SAS Institute, Cary, NC, USA version 8.2, TS2M0).

Results

Groups were comparable at baseline for the risk factors previously identified for predicting radiological progression in the DMARDs group (Table 1). As shown in Figs. 1 and 2, differences in the 1-year changes in radiological erosion and JSN scores between patients in the DMARDs and tocilizumab monotherapy arms varied between subgroups divided according to the baseline levels of each predictive marker for radiographically evident joint damage (uCTX-II, uPYD/DPD, JSN, and BMI). The 1-year changes in radiological erosion scores in patients with high uCTX-II, high uPYD/DPD, or low BMI at baseline, indicating a high risk of progressive joint erosion, were significantly lower in tocilizumab-treated than in DMARD-treated patients (Fig. 1). Those changes in radiological JSN scores in patients with high uCTX-II, high uPYD/DPD, high JSN, or low BMI at baseline, indicating a high risk of progressive JSN, were also lower in tocilizumab-treated than in DMARD-treated patients (Fig. 2a–d), and there were proven to be significant differences in cases with high JSN and low BMI (Fig. 2c, d). In contrast, low-risk patients receiving tocilizumab monotherapy progressed less than patients on DMARDs, although the differences were very small and did not reach statistical significance (Figs. 1 and 2).

Discussion

Biological agents targeting inflammatory cytokines are more effective at suppressing progression of joint damage than are conventional DMARDs. However, previously reported studies on the efficacies of these agents for slowing radiological damage showed that there was still significant progression in many patients [1–11]. These data allowed us to recognize that many patients on nonbiologic DMARDs show no radiographic progression, and some even show radiographic improvement. Specifically, our previous data showed that 39% of patients treated with conventional DMARDs showed no radiographic progression in 1-year follow-up [10]. However, biological agents may have side effects. With such knowledge gained from growing experience in the use of biologics, patients would benefit from personalized therapies based on accurate prognostic tools rather than standard therapies that do not evaluate risk factor to guide treatment selection. A better understanding of the prognostic factors for progressive joint damage under nonbiological treatment and appropriate targeting of biologics to patients with RA at high risk of progressive joint damage and disability could enhance risk–benefit balance of RA therapeutic strategies. Thus, many investigators have sought such prognostic factors. Young-Min et al. reported the possible usefulness of matrix metalloproteinase-3 (MMP-3) and uCTX-II in predicting radiographic outcome in RA patients treated with DMARDs [14], and Charni et al. reported the possible usefulness of urinary type II collagen helical peptide (HELIX-II) [15]. We found that high baseline levels of uCTX-II, uPYD/DPD, JSN score, and low BMI were independently significantly associated with 1-year progression of joint destruction under conventional DMARDs treatment [12]. Most of these newly developed or recognized markers are still not widely used in clinical practice; however, further understanding the significance of these markers would facilitate better therapies. Having established these risk factors, the efficacy of biologics for

Table 1 Baseline values in the different patient groups

Variables	Cutoff value	DMARDs $N = 145$		Tocilizumab $N = 157$	
		N	Mean of baseline value ± SD	*N*	Mean of baseline value ± SD
JSN	0	30	0	32	0
	>0	115	21.1 ± 22.5	125	18.2 ± 21.8
uCTX-II (ng/mmol/creatinine)	<500	53	327.2 ± 104.6	66	337.0 ± 102.9
	≥500	88	1249.0 ± 1014.9	83	1156.0 ± 585.8
uPYD/DPD	<6.8	72	5.8 ± 0.7	76	5.5 ± 0.8
	≥6.8	73	8.6 ± 1.4	81	8.5 ± 1.3
BMI (kg/m^2)	<18.5	20	17.5 ± 1.2	26	17.5 ± 0.6
	≥18.5 and <25	102	21.5 ± 1.6	102	21.5 ± 1.8
	≥25	21	27.1 ± 1.7	29	28.2 ± 2.4

Criteria were according to criteria of the World Health Organization [16] employees

JSN joint space narrowing, *uPYD/DPD* urinary pyridinoline/deoxypyridinoline ratio, *uCTX-II* urinary C-terminal telopeptide of type II collagen, *BMI* body mass index, *SD* standard deviation

BMI <18.5, underweight; ≥18.5 and <25, normal weight; 25≤, overweight or obese

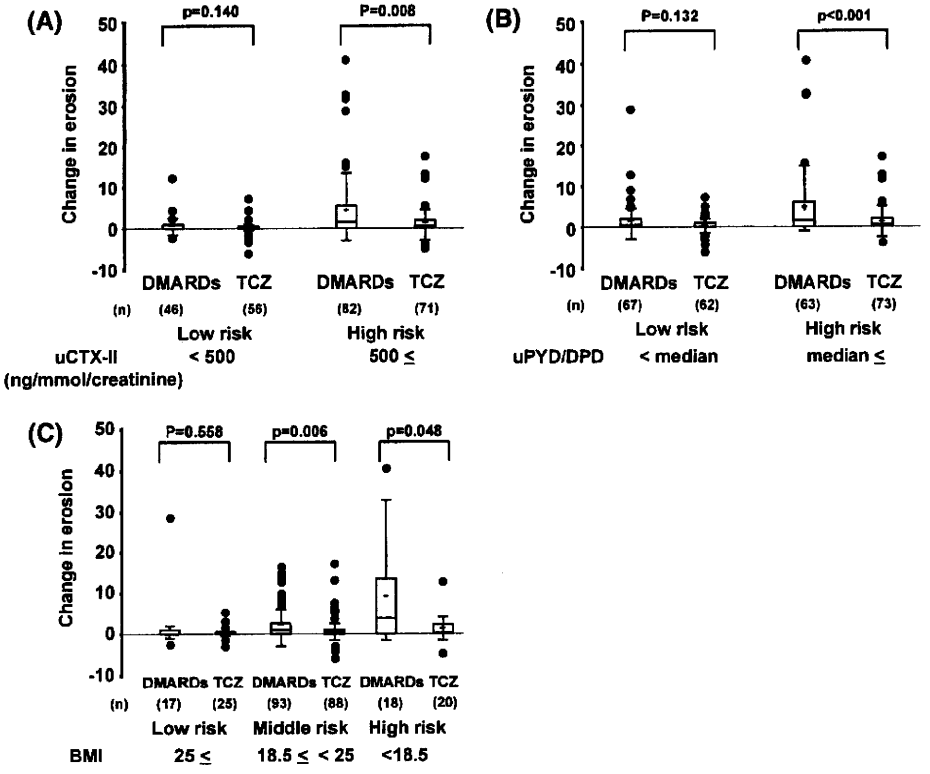

Fig. 1 One-year change of erosion scores in tocilizumab-treated rheumatoid arthritis (RA) patients at high risk for developing erosions. One-year change in erosion scores were analyzed for individual risk factors (**a** uCTX, **b** uPYD/DPD, **c** BMI) at baseline. Results are expressed as median (*line* across *boxes*), 25–75% interquartile range (*boxes*), mean (*cross symbol* in *boxes*), standard deviation (SD) (*vertical line* across the *top of the box*), and standard error (*vertical line* across *bottom of the box*). The *filled circles* represent individual values over SD values. Differences in changes in erosion scores were compared by the Wilcoxon rank sum test. *uPYD/DPD* urinary pyridinoline/deoxypyridinoline ratio, *uCTX-II* urinary C-terminal telopeptide of type II collagen, *BMI* body mass index, *TCZ* tocilizumab

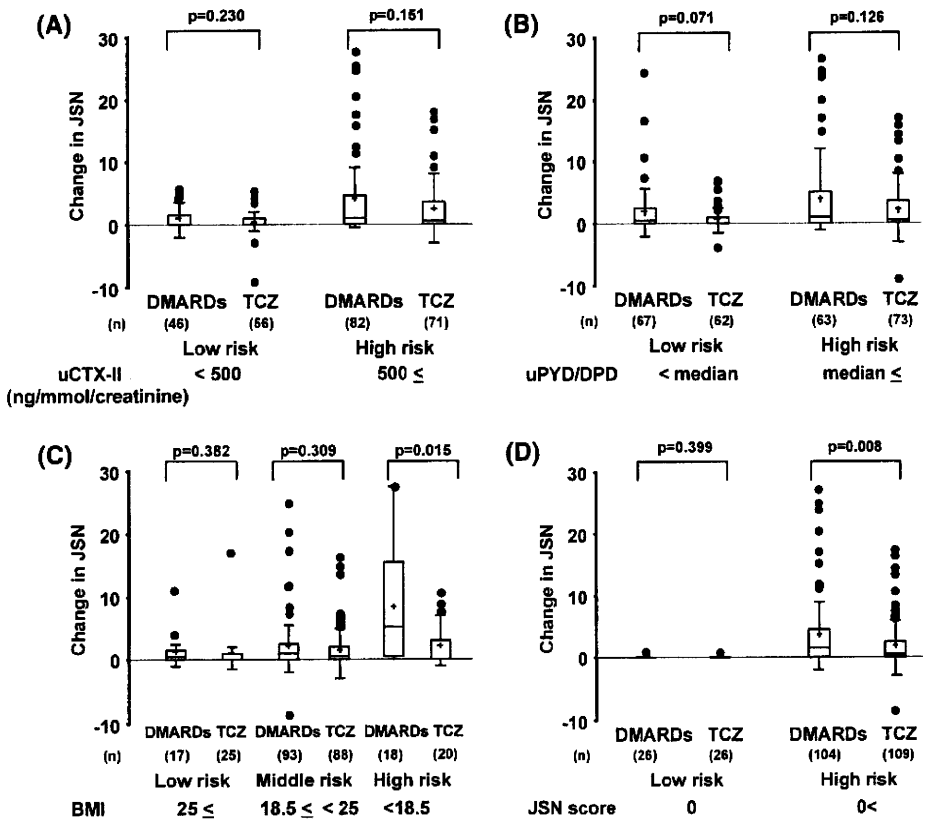

Fig. 2 One-year change of joint space narrowing (JSN) scores in tocilizumab-treated rheumatoid arthritis (RA) patients with risk factors for developing JSN. Score changes were analyzed for individual risk factors (**a** uCTX, **b** uPYD/DPD, **c** BMI, **d** JSN) at baseline. Results are expressed as median (*line* across *boxes*), 25–75% interquartile range (*boxes*), mean (*cross symbol* in *boxes*), standard deviation (SD) (*vertical line* across *top of the box*), and standard error (*vertical line* across *bottom of the box*). The *filled circles* represent individual values over SD values. Differences in change in JSN scores were compared by the Wilcoxon rank sum test. *uPYD/DPD* urinary pyridinoline/deoxypyridinoline ratio, *uCTX-II* urinary C-terminal telopeptide of type II collagen, *BMI* body mass index, *TCZ* tocilizumab

reducing joint destruction in high-risk groups needed to be confirmed to effectively target treatment. Therefore, in this study, subanalysis from a prospective 1-year randomized controlled trial of tocilizumab (SAMURAI trial) was performed to investigate the ability of this agent to reduce progression of structural joint damage in high-risk patients. There was no significant difference in 1-year changes of JSN scores between DMARD- and tocilizumab-treated patients in high-risk groups, as estimated by high uCTX-II, uPYD/DPD. Our data show, however, that tocilizumab monotherapy effectively blocked progression of bone erosion in all high-risk groups as estimated by high uCTX-II, uPYD/DPD, or low BMI and also effectively blocked progression of JSN in high-risk groups as estimated by low BMI or high JSN score, The differences in 1-year changes of erosion and JSN scores between the DMARD- and tocilizumab-treated patients were greatest in the high-risk groups, whereas there was little to no difference in the low-risk group. These findings indicate that the benefit of tocilizumab monotherapy to inhibit bone erosion and JSN progression is maximized in high-risk groups as estimated by high uCTX-II, uPYD/DPD, or low BMI, and by low BMI or high JSN score, respectively. To our knowledge, this is the first comprehensive report showing the usefulness of biomarker targeting strategies for biologics in treating RA. There were smaller and nonsignificant differences in 1-year changes of erosion and JSN scores between patients in the DMARD or tocilizumab monotherapy treatment groups in the low-risk category, although progression was still lower in individuals receiving tocilizumab. The lack of statistical significance can be due in part to the very limited progression in the low-risk group reducing the power to detect differences. These findings also suggest that patients at low risk may benefit less from treatment with biologics unless they develop changes in markers that indicate an increased risk of progression during treatment with conventional DMARDs. On the other hand, the lack of statistically significant differences in 1-year changes of JSN scores between patients in the DMARD or tocilizumab monotherapy treatment groups in the high-risk category might be due to the relatively weak prognostic power of high uCTX-II and uPYD/DPD for JSN progression compared with low BMI or high JSN score [12].

Establishing means of early discrimination between tocilizumab radiological responders and nonresponders is therefore raised as the next issue to be addressed when considering targeted therapeutic strategies. In conclusion, we demonstrated that tocilizumab monotherapy is effective in reducing radiological progression in patients presenting with risk factors for rapid progression of joint damage.

Acknowledgments This work was supported by Chugai Pharmaceutical Co., Ltd., Tokyo, Japan.

Conflict of interest statement NN has served as a consultant to and received honoraria from Chugai Pharmaceutical Co. Ltd., the manufacturer of TCZ. NN also works as a scientific advisor to F. Hoffmann-La Roche, which is developing TCZ in collaboration with Chugai Pharmaceutical Co., Ltd.

References

1. Lipsky PE, van der Heijde DM, St Clair EW, Furst DE, Breedveld FC, Kalden JR, et al. Infliximab and methotrexate in the treatment of rheumatoid arthritis. Anti-Tumor Necrosis Factor Trial in Rheumatoid Arthritis with Concomitant Therapy Study Group. N Engl J Med. 2000;343(22):1594–602.
2. Bathon JM, Martin RW, Fleischmann RM, Tesser JR, Schiff MH, Keystone EC, et al. A comparison of etanercept and methotrexate in patients with early rheumatoid arthritis. N Engl J Med. 2000; 343(22):1586–93.
3. Klareskog L, van der Heijde D, de Jager JP, Gough A, Kalden J, Malaise M, et al. Therapeutic effect of the combination of etanercept and methotrexate compared with each treatment alone in patients with rheumatoid arthritis: double-blind randomised controlled trial. Lancet. 2004;363(9410):675–81.
4. St Clair EW, van der Heijde DM, Smolen JS, Maini RN, Bathon JM, Emery P, et al. Combination of infliximab and methotrexate therapy for early rheumatoid arthritis: a randomized, controlled trial. Arthritis Rheum. 2004;50(11):3432–43.
5. Keystone EC, Kavanaugh AF, Sharp JT, Tannenbaum H, Hua Y, Teoh LS, et al. Radiographic, clinical, and functional outcomes of treatment with adalimumab (a human anti-tumor necrosis factor monoclonal antibody) in patients with active rheumatoid arthritis receiving concomitant methotrexate therapy: a randomized, placebo-controlled, 52-week trial. Arthritis Rheum. 2004;50(5): 1400–11.
6. Genovese MC, Bathon JM, Fleischmann RM, Moreland LW, Martin RW, Whitmore JB, et al. Longterm safety, efficacy, and radiographic outcome with etanercept treatment in patients with early rheumatoid arthritis. J Rheumatol. 2005;32(7):1232–42.
7. van der Heijde D, Landewe R, Klareskog L, Rodriguez-Valverde V, Settas L, Pedersen R, et al. Presentation and analysis of data on radiographic outcome in clinical trials: experience from the TEMPO study. Arthritis Rheum. 2005;52(1):49–60.
8. van der Heijde D, Klareskog L, Rodriguez-Valverde V, Codreanu C, Bolosiu H, Melo-Gomes J, et al. Comparison of etanercept and methotrexate, alone and combined, in the treatment of rheumatoid arthritis: two-year clinical and radiographic results from the TEMPO study, a double-blind, randomized trial. Arthritis Rheum. 2006;54(4):1063–74.
9. Breedveld FC, Weisman MH, Kavanaugh AF, Cohen SB, Pavelka K, van Vollenhoven R, et al. The PREMIER study: a multicenter, randomized, double-blind clinical trial of combination therapy with adalimumab plus methotrexate versus methotrexate alone or adalimumab alone in patients with early, aggressive rheumatoid arthritis who had not had previous methotrexate treatment. Arthritis Rheum. 2006;54(1):26–37.
10. Nishimoto N, Hashimoto J, Miyasaka N, Yamamoto K, Kawai S, Takeuchi T, et al. Study of active controlled monotherapy used for rheumatoid arthritis, an IL-6 inhibitor (SAMURAI): evidence of clinical and radiographic benefit from an x ray reader-blinded randomised controlled trial of tocilizumab. Ann Rheum Dis. 2007;66(9):1162–7.
11. Genant HK, Peterfy CG, Westhovens R, Becker JC, Aranda R, Vratsanos G, et al. Abatacept inhibits progression of structural

damage in rheumatoid arthritis: results from the long-term extension of the AIM trial. Ann Rheum Dis. 2008;67(8):1084–9.
12. Hashimoto J, Garnero P, van der Heijde D, Miyasaka N, Yamamoto K, Kawai S, et al. A combination of biochemical markers of cartilage and bone turnover, radiographic damage and body mass index to predict the progression of joint destruction in patients with rheumatoid arthritis treated with disease-modifying anti-rheumatic drugs. Mod Rheumatol. 2009;19(3):273–82.
13. van der Heijde D. How to read radiographs according to the Sharp/van der Heijde method. J Rheumatol. 2000;27(1):261–3.
14. Young-Min S, Cawston T, Marshall N, Coady D, Christgau S, Saxne T, et al. Biomarkers predict radiographic progression in early rheumatoid arthritis and perform well compared with traditional markers. Arthritis Rheum. 2007;56(10):3236–47.
15. Charni N, Juillet F, Garnero P. Urinary type II collagen helical peptide (HELIX-II) as a new biochemical marker of cartilage degradation in patients with osteoarthritis and rheumatoid arthritis. Arthritis Rheum. 2005;52(4):1081–90.
16. World Health Organization. Diet, nutrition and the prevention of chronic diseases. Report of a joint WHO/FAO expert consultation, January 28–February 1, 2002. Geneva: WHO; 2003. http://www.fao.org/DOCREP/005/AC911E/AC911E00.HTM

Bone 48 (2011) 476–484

Contents lists available at ScienceDirect

Bone

journal homepage: www.elsevier.com/locate/bone

PKCα suppresses osteoblastic differentiation

Akio Nakura, Chikahisa Higuchi *, Kiyoshi Yoshida, Hideki Yoshikawa

Department of Orthopaedic Surgery, Graduate School of Medicine, Osaka University, Suita, Osaka, Japan

ARTICLE INFO

Article history:
Received 11 May 2010
Revised 8 September 2010
Accepted 29 September 2010
Available online 14 October 2010

Edited by: Toshio Matsumoto

Keywords:
PKCα
MC3T3-E1 cells
Osteoblastic differentiation
Osteoblastic cell proliferation
Signal transduction

ABSTRACT

Protein kinase C (PKC) plays an essential role in cellular signal transduction for mediating a variety of biological functions. There are 11 PKC isoforms and these isoforms are believed to play distinct roles in cells. Although the role of individual isoforms of PKC has been investigated in many fields, little is known about the role of PKC in osteoblastic differentiation. Here, we investigated which isoforms of PKC are involved in osteoblastic differentiation of the mouse preosteoblastic cell line MC3T3-E1. Treatment with Gö6976, an inhibitor of PKCα and PKCβI, increased alkaline phosphatase (ALP) activity as well as gene expression of ALP and Osteocalcin (OCN), and enhanced calcification of the extracellular matrix. Concurrently, osteoblastic cell proliferation decreased at a concentration of 1.0 μM. In contrast, a PKCβ inhibitor, which inhibits PKCβI and PKCβII, did not significantly affect osteoblastic differentiation or cell proliferation. Knockdown of PKCα using MC3T3-E1 cells transfected with siRNA also induced an increase in ALP activity and in gene expression of ALP and OCN. In contrast, overexpression of wild-type PKCα decreased ALP activity and attenuated osteoblastic differentiation markers including ALP and OCN, but promoted cell proliferation. Taken together, our results indicate that PKCα suppresses osteoblastic differentiation, but promotes osteoblastic cell proliferation. These results imply that PKCα may have a pivotal role in cell signaling that modulates the differentiation and proliferation of osteoblasts.

Introduction

Protein kinase C (PKC) is a serine/threonine protein kinase that is known to be involved in multiple cellular signal transduction pathways that mediate cellular functions such as proliferation and differentiation [1–4]. PKC was first purified from bovine cerebellum in 1977 as a new species of protein kinase [5], following which, it was shown to be expressed in many other tissues [6]. To date, 11 PKC isoforms have been identified, which are classified into three groups based on their structure and cofactor regulation [7,8]: conventional PKC (α, βI, βII, and γ), novel PKC (δ, ε, η, θ, and μ), and atypical PKC (ζ and λ). Conventional PKCs are Ca^{2+}-dependent and are activated by both phosphatidylserine (PS) and the second messenger diacylglycerol (DAG). Novel PKCs are regulated by PS and DAG, but their activation is Ca^{2+}-independent. Atypical PKCs require neither Ca^{2+} nor PS and DAG for activation. Although some PKC isoforms are cell-type specific, PKCα, δ, ε, and ζ seem to be ubiquitous [7,9].

The role of each PKC isoform has been mostly evaluated in a variey of fields using genetic and molecular approaches employing isoform-specific inhibitors [10–12], isoform-specific RNAi and/or isoform overexpression. Much progress has been made in clinical studies of the role of PKC isoforms in cardiovascular disease and tumorigenesis and some isoforms of PKC are currently being used as theraupic targets [13]. For example, a selective inhibitor of PKCβ is under evaluation in a clinical trial as a theraupic agent for diabetic complications [14,15]. Although such systemic diseases often involve a change in bone quantity and quality, little is known about the effects of PKC on bone formation. Expression of PKC isoforms in osteoblasts has been reported [4,16], suggesting that a therapeutic agent targeted towards specific PKC isoforms might inadvertently modulate bone formation. Conversely, if the involvement of isoforms of PKC in bone formation are understood, a new agent for the regulation of bone formation might be developed.

Our purpose was to determine which isoforms of PKC play an important role in osteoblastic differentiation. In the present paper, we mainly investigated the role of PKCα and PKCβ in osteoblasts using commercially available inhibitors of PKC isoforms. We speculated that of the eleven different isoforms of PKC, PKCα in particular may have a suppressive role in osteoblastic differentiation. In addition, we confirmed this role of PKCα by knockdown of PKCα, and by overexpression of PKCα, in MC3T3-E1 cells. Meanwhile, PKCα promoted osteoblastic proliferation. Our present study indicates that PKCα suppresses osteoblastic differentiation.

* Corresponding author. Department of Orthopaedic Surgery, Graduate School of Medicine, Osaka University, 2-2 Yamadaoka, Suita, Osaka 565-0871, Japan. Fax: +81 6 6879 3559.
E-mail addresses: nakura-osaka@umin.ac.jp (A. Nakura), c-higuchi@umin.ac.jp (C. Higuchi), y_kiyoshi@csc.jp (K. Yoshida), yhideki@ort.med.osaka-u.ac.jp (H. Yoshikawa).

8756-3282/$ – see front matter © 2010 Elsevier Inc. All rights reserved.
doi:10.1016/j.bone.2010.09.238

Materials and methods

Cell culture

Mouse preosteoblastic MC3T3-E1 cells were obtained from Riken Cell Bank (Tsukuba, Japan). The cells were seeded at a concentration of 2.0×10^4 cells/cm^2 in α-minimal essential medium (α-MEM; Invitrogen, Carlsbad, CA, USA) supplemented with 10% fetal bovine serum (FBS; Hyclone, Road Logan, UT, USA) (growth medium) at 37 °C under a humidified atmosphere of 5% CO_2. For each assay, the growth medium was replaced with growth medium supplemented with 0.2 mM ascorbic acid (AA; Sigma-Aldrich, St. Louis, MO, USA) and 10 mM β-glycerophosphate (βGP; Sigma-Aldrich) (differentiation medium). The medium was changed twice per week.

Alkaline phosphatase (ALP) staining

MC3T3-E1 cells were seeded in a 24-well plate at a density of 2.0×10^4 cells/cm^2. After 24 h incubation, the cells were treated with the PKCα/PKCβI inhibitor Gö6976 (Calbiochem, San Diego, CA, USA), the PKCβ inhibitor (Calbiochem), or with 12-O-tetradecanoylphorbol-13-acetate (TPA; Calbiochem) in differentiation medium for 3 days. For ALP staining, cells were washed with phosphate-buffered saline (PBS; Sigma-Aldrich) and fixed for 15 min with 10% formalin at room temperature. After fixation, the cells were incubated with the ProtoBlot® II AP System with Stabilized Substrate (Promega, Madison, WI, USA) for 1 h at room temperature. For all experiments using inhibitors and activators of PKC, we also assayed the vehicle (DMSO) as a standard control [17].

ALP activity

To measure ALP activity, cells were washed twice with PBS and then lysed in mammalian protein extraction reagent (M-PER; Pierce, Rockford, IL, USA) following the manufacturer's protocol. ALP activity was measured using LabAssay™ ALP (Wako Pure Chemicals Industries, Ltd., Osaka, Japan) and p-nitrophenylphosphate as a substrate. In order to normalize enzyme activity, the protein content was measured using a bichinconinic acid (BCA) protein assay kit (Pierce).

Proliferation assay

MC3T3-E1 cells were cultured in 48-well plates at a concentration of 2.0×10^4 cells/cm^2 in differentiation medium. Cell proliferation was assessed using the Premix WST-1 cell proliferation assay system (Takara Bio, Inc., Otsu, Japan) according to the manufacturer's instructions. We performed this assay every 24 h.

Alizarin red staining

MC3T3-E1 cells were cultured for 28 days on BIOCOAT® 24-well plates (Nippon Becton Dickinson Co., Ltd., Tokyo, Japan) in differentiation medium. Then, the cells were washed twice with PBS, fixed in 10% formalin for 10 min and then stained with Alizarin Red S (Sigma-Aldrich) at pH 6.3 for 1 h. After discarding the Alizarin Red S solution and washing the cells three times with distilled water, bound Alizarin Red was dissolved in 200 μL of 100 mM hexadecylpyridium chloride (Sigma-Aldrich) and the absorbance of the supernatant was measured at 570 nm.

Reverse transcription PCR (RT-PCR) and quantitative real-time PCR

Total RNA was isolated from cells using TRIzol (Invitrogen) according to the manufacturer's instructions. cDNA was synthesized using the Transcriptor First Strand cDNA Synthesis kit (Roche Diagnostics GmbH, Mannheim, Germany). RT-PCR was performed using a PCR Master Mix (Promega) and an appropriate pair of primers. The sequences of the specific primers used for RT-PCR are shown in Table 1. PCR products were separated by agarose gel electrophoresis and stained with ethidium bromide. Each mRNA was measured using a quantitative real-time PCR assay, which employed LightCycler® TaqMan® Master (Roche Diagnostics), a Universal ProbeLibrary Probe (UPL Probe; Roche Diagnostics), an appropriate pair of primers according to the manufacturer's protocol. The sequences of specific primers and UPL Probes used are shown in Table 2. Expression values were normalized to GAPDH.

Western blotting

The cells were rapidly lysed on ice using Blue Loading Buffer Reagents (Cell Signaling Technology, Beverly, MA, USA) containing 0.125 M dithiothreitol. These samples were subjected to 8% SDS-PAGE and were then transferred onto nitrocellulose membranes (Bio-Rad Laboratories, Inc., Hercules, CA, USA). After blocking with 0.1% Tween-added PBS (T-PBS) containing 3% bovine serum albumin (BSA; Sigma-Aldrich), the membranes were incubated with specific primary antibodies against PKCα (Cell Signaling Technology), PKCβ (Abnova Co., Ltd., Taipei, Taiwan), PKCβII (Santa Cruz Biotechnology, Inc., Austin, TX, USA), and β-actin (Sigma-Aldrich). Horseradish peroxidase-conjugated anti-mouse or -rabbit secondary antibody (GE Healthcare, UK) were incubated for 1 h at room temperature in 0.1% T-PBS. The blots were visualized by enhanced chemiluminescence substrate (Thermo Scientific, Rockford, IL, USA) using a Western blotting detection system.

Knockdown of PKCα using RNA interference

MC3T3-E1 cells were transfected with small interfering RNA (siRNA) using Lipofectamine RNAiMAX (Invitrogen) according to the manufacturer's protocol. Two different sets of PKCα siRNA oligos were used for knockdown of PKCα: site 1 (5′-GGAUUUAUCUGAAGGCUGA-3′ and 5′-UCAGCCUUCAGAUAAAUCC-3′) and site 2 (5′-GCAAAGGACUUAUGAC-CAA-3′ and 5′-UUGGUCAUAAGUCCUUUGC-3′) (B-Bridge International, Inc., Sunnyvale, CA, USA). Control siRNA was purchased from B-Bridge International, Inc. MC3T3-E1 cells transfected with siRNA were seeded in a 24-well plate at a concentration of 1.0×10^4 cells/cm^2 for 48 h. The medium was then replaced with differentiation medium and the cells were incubated for 3 days prior to use for experiments.

Infection with adenovirus vectors

Adenovirus expressing rabbit PKCα, rabbit PKCβII, and β-galactosidase were generous gifts from Dr. M. Ohba, Tokyo, Japan [18]. Each recombinant adenovirus was plaque purified, expanded, and titered

Table 1
Sequences of PCR primers and specific probes used for quantitative real-time PCR.

Gene	UPL probe no.	Primer	Sequence (5′→3′)
ALP	81	Forward	ACTCAGGGCAATGAGGTCAC
		Reverse	CACCCGAGTGGTAGTCACAA
Osteocalcin	71	Forward	CACCATGAGGACCCTCTCTC
		Reverse	TGGACATGAAGGCTTTGTCA
Collagen type 1 a1	15	Forward	CATGTTCAGCTTTGTGGACCT
		Reverse	GCAGCTGACTTCAGGGATGT
Runx2	34	Forward	GCCCAGGCGTATTTCAGAT
		Reverse	TGCCTGGCTCTTCTTACTGAG
Osterix	106	Forward	CTCCTGCAGGCAGTCCTC
		Reverse	GGGAAGGGTGGGTAGTCATT
GAPDH	80	Forward	TGTCCGTCGTGGATCTGAC
		Reverse	CCTGCTTCACCACCTTCTTG